The *NRC0* gene cluster of sensor and helper NLR immune receptors is functionally conserved across asterid plants

Toshiyuki Sakai[1,2], Claudia Martinez-Anaya[1,3], Mauricio P Contreras[1], Sophien Kamoun[1*], Chih-Hang Wu[1,4*], Hiroaki Adachi[1,2,5*]

[1]The Sainsbury Laboratory, University of East Anglia, Norwich Research Park, NR4 7UH, Norwich, UK

[2]Laboratory of Crop Evolution, Graduate School of Agriculture, Kyoto University, Mozume, Muko, Kyoto 617-0001, Japan

[3]Instituto de Biotecnología, Universidad Nacional Autónoma de México, 62110, Cuernavaca, Morelos, México

[4]Institute of Plant and Microbial Biology, Academia Sinica, Nankang, Taipei 11529, Taiwan

[5]JST-PRESTO, 4-1-8, Honcho, Kawaguchi, Saitama 332-0012, Japan

Correspondence: Sophien.Kamoun@TSL.ac.uk; wuchh@gate.sinica.edu.tw; adachi.hiroaki.3s@kyoto-u.ac.jp

Short title: Conserved NRC-clade gene cluster in asterids

One-sentence summary: *NRC0* gene cluster is functionally conserved across divergent asterid species and predates the massively expanded NRC network.

ABSTRACT

NLR (nucleotide-binding domain and leucine-rich repeat-containing) proteins can form complex receptor networks to confer innate immunity. NRCs are phylogenetically related nodes that function downstream of a massively expanded network of disease resistance proteins that protect against multiple plant pathogens. Here, we used phylogenomic methods to reconstruct the macroevolution of the NRC family. One of the NRCs, we termed *NRC0*, is the only family member shared across asterid plants, leading us to investigate its evolutionary history and genetic organization. In several asterid species, *NRC0* is genetically clustered to other NLRs that are phylogenetically related to NRC-dependent disease resistance genes. This prompted us to hypothesize that the ancestral state of the NRC network is an NLR helper-sensor gene cluster that was present early during asterid evolution. We validated this hypothesis by demonstrating that NRC0 is essential for the hypersensitive cell death induced by its genetically linked sensor NLR partners in four divergent asterid species: tomato, wild sweet

36   potato, coffee and carrot. In addition, activation of a sensor NLR leads to high-order complex

37   formation of its genetically linked NRC0 similar to other NRCs. Our findings map out

38   contrasting evolutionary dynamics in the macroevolution of the NRC network over the last 125

39   million years from a functionally conserved NLR gene cluster to a massive genetically

40   dispersed network.

41

42   *Keywords: plant immunity // host-pathogen interaction // disease resistance gene // nucleotide-binding*

43   *domain and leucine-rich repeat–containing protein // pathogen effector // NLR-mediated immunity //*

44   *immune receptor network // evolution*

45

46   **INTRODUCTION**

47   Plants have evolved an effective innate immune system that is activated by immune receptors

48   upon sensing diverse pathogen molecules in either the extracellular or intracellular space of

49   host cells. One such immune receptor is the nucleotide-binding domain and leucine-rich repeat-

50   containing protein (NLR) family, composed of intracellular immune receptors recognizing

51   pathogen-secreted proteins called effectors (Jones et al., 2016). The evolution of NLRs is

52   marked by a continuous arms race between plants and pathogens, leading to the rapid evolution

53   and diversification of NLR genes even at the intraspecific level (Van de Weyer et al., 2019;

54   Lee and Chae, 2020; Prigozhin and Krasileva, 2021). NLRs are known as the most diverse

55   protein family in flowering plants, as many plants have hundreds to thousands of diverse NLR

56   genes in their genomes (Shao et al., 2016; Baggs et al., 2017; Kourelis et al., 2021). This

57   diversification and expansion of NLR genes in plants possibly occurred through genome

58   rearrangements such as gene duplication, deletion and conversion, as well as point mutations

59   and domain insertions (Barragan and Weigel, 2021). As a consequence of these events, NLR

60   genes in plant genomes are often found in clusters. For example, in *Arabidopsis thaliana*

61   accessions, 47 to 71% of NLR genes form NLR gene clusters in their genomes (Van de Weyer

62   et al., 2019). Clustered NLR genes tend to have higher nucleotide sequence diversity than non-

63   clustered NLR genes in Arabidopsis (Van de Weyer et al., 2019), thereby providing a reservoir

64   of genetic variation for novel immune specificities against fast-evolving pathogen effectors.

65   Understanding the macroevolutionary dynamics of NLRs across diverse plant species is crucial

66   not only for unraveling the molecular mechanisms underlying plant immunity but also for

67   providing genetic resources of disease resistance traits for global food security.

68

69   NLR and NLR-related proteins are key components of innate immunity and non-self
70   recognition not only in plants but also in animals, fungi and bacteria (Jones et al., 2016; Uehling
71   et al., 2017; Kibby et al., 2023). Plant NLRs have a shared domain architecture of a central
72   nucleotide-binding domain with APAF-1, various R proteins, and CED-4 (NB-ARC) domain
73   and a C-terminal leucine-rich repeat (LRR) domain (Kourelis et al., 2021). At the N-terminal
74   region of plant NLRs, there is a variable domain that can be a coiled-coil (CC) or a
75   toll/Interleukin-1 Receptor (TIR) domain. Based on the N-terminal domains, plant NLRs are
76   broadly classified into four subfamilies: CC-NLRs (CNLs), G10-type CC-NLRs (CC_{G10}-
77   NLRs), RESISTANCE TO POWDERY MILDEW 8 (RPW8)-type CC-NLRs (CC_R-NLRs or
78   RNLs) and TIR-NLRs (TNLs) (Lee et al., 2021). Phylogenomic studies revealed that the most
79   widely conserved CC-NLR gene across flowering plant (angiosperm) species is *HOPZ-
80   ACTIVATED RESISTANCE1* (*ZAR1*), which was initially identified in Arabidopsis (Gong et
81   al., 2022; Adachi et al., 2023). As there is no NLR gene genetically clustered to the *ZAR1* locus
82   across angiosperm species, *ZAR1* is defined as a genetic singleton NLR gene throughout its
83   evolution, and indeed the ZAR1 protein functions as a singleton NLR that doesn't appear to
84   require other NLRs to activate immunity (Adachi et al., 2023). Upon effector recognition
85   through its LRR domain and partner receptor-like cytoplasmic kinases (RLCKs), activated
86   ZAR1 forms a homo-pentameric complex called "resistosome", that functions as a calcium ion
87   (Ca^{2+}) channel at the plasma membrane that is required for induction of the hypersensitive cell
88   death immune response (Wang et al., 2019a; Wang et al., 2019b; Bi et al., 2021). To make a
89   pore on the plasma membrane and cause Ca^{2+} influx, the ZAR1 resistosome exposes a funnel-
90   shaped structure formed by its first α helix (α1 helix) of the N-terminal CC domain (Wang et
91   al., 2019b; Bi et al., 2021). The α1 helix was defined as the "MADA motif" that is conserved
92   in about 20% of CC-NLRs from dicot and monocot species (Adachi et al., 2019a). The MADA
93   sequence is functionally interchangeable between dicot and monocot CC-NLRs, suggesting a
94   conserved immune activation mechanism by MADA-type CC-NLRs across angiosperms.
95   Indeed, upon effector perception, the MADA-type CC-NLR Sr35 in wheat forms the homo-
96   oligomerized resistosome complex and causes Ca^{2+} influx (Förderer et al., 2022).

97

98   Although some plant NLRs operate as singletons, many plant NLRs have functionally
99   specialized to recognize pathogen effectors (sensor NLRs) or to activate immune responses
100   (helper NLRs, also known as executor NLRs) (Adachi et al., 2019b; Kourelis and Adachi,
101   2022). Interestingly, these functionally specialized NLRs often form gene pairs or clusters in
102   plant genomes and function together in immune activation and regulation. For example, in

103   Arabidopsis, *RESISTANCE TO RALSTONIA SOLANACEARUM 1* (*RRS1*) / *RESISTANCE TO*

104   *PSEUDOMONAS SYRINGAE 4* (*RPS4*) (Narusaka et al., 2009; Sarris et al., 2015; Le Roux et

105   al., 2015), *Chilling Sensitive 1* (*CHS1*) / *Suppressors of chs1-2, 3* (*SOC3*) and *TIR-NB 2* (*TN2*)

106   (Zhang et al., 2017; Liang et al., 2019), *CONSTITUTIVE SHADE-AVOIDANCE 1* (*CSA1*) /

107   *CHILLING SENSITIVE 3* (*CHS3*) (Xu et al., 2015; Yang et al., 2022), *SUPRESSOR OF NPR1,*

108   *CONSTITUTIVE 1* (*SNC1*) / *SIDEKICK SNC1 1* (*SIKIC1*), *SIKIC2* and *SIKIC3* (Dong et al.,

109   2018), form genetically linked pairs or clusters that function together in immune responses. In

110   rice, *RESISTANCE GENE ANALOG 5* (*RGA5*) / *RGA4* and *PYRICULARIA ORYZAE*

111   *RESISTANCE K-1* (*Pik-1*) / *Pik-2* are two sensor-helper NLR pairs that are found in head-to-

112   head orientation in the genome (Césari et al., 2014; Maqbool et al., 2015; Shimizu et al., 2022;

113   Sugihara et al., 2023).

114

115   In addition to NLR pairs, genetically dispersed NLRs often function together and form complex

116   immune receptor networks. In solanaceous plants, CC-NLR proteins known as NLR-

117   REQUIRED FOR CELL DEATH (NRC) function as helper NLRs (NRC-H) for multiple

118   sensor NLRs (NRC-S) to mediate immune responses and to confer disease resistance against

119   diverse pathogens (Wu et al., 2017). Although NRC-H and NRC-S genes are phylogenetically

120   linked and form a hugely expanded NRC superclade, NRC-H and NRC-S genes are scattered

121   throughout the genome of solanaceous plants (Wu et al., 2017). Recent biochemical and cell

122   biology studies revealed that activated NRC-S induce homo-oligomerization of NRC-H, and

123   activated NRC-H form punctate structures at the plasma membrane (Duggan et al., 2021;

124   Contreras et al., 2023a; Contreras et al., 2023b; Ahn et al., 2023). This suggests that in NRC

125   networks, NRC-H proteins activated by NRC-S presumably trigger immune responses at the

126   plasma membrane, as is the case in the ZAR1 resistosome model. Consistent with this view,

127   NRC-H in the NRC superclade have the MADA motif at their N-termini (Adachi et al., 2019a).

128   In contrast, the N-termini of NRC-S genes have diversified and/or acquired additional

129   extension domains prior to the CC domain (Adachi et al., 2019a; Seong et al., 2020). Based on

130   these findings, a current evolutionary model of the NRC network is that NRC-H and NRC-S

131   evolved from a multifunctional singleton NLR and have functionally specialized into helper

132   and sensor NLRs throughout evolution (Adachi et al., 2019b; Adachi and Kamoun, 2022).

133

134   In a previous study, the NRC network was proposed to have evolved from a sensor–helper gene

135   cluster (Wu et al., 2017). Outside of the asterid lineages, the Caryophyllales species *Beta*

136   *vulgaris* (sugar beet) encodes one NRC helper and two NRC sensor genes that form a gene

137   cluster (Wu et al., 2017). Therefore, the NRC superclade presumably emerged from a pair of

138   genetically linked NLRs about 100 million years ago (mya) before the asterids and

139   Caryophyllales lineages split. However, our knowledge of how NRC networks evolved across

140   asterids and other Solanaceae-related plant species remains limited. In particular, the

141   evolutionary dynamics of the NRC helpers across the asterids have not been studied in detail.

142   Here, we show that *NRC0* is the only NRC-H family member that has remained conserved

143   across asterid species. *NRC0* orthologs form gene pairs or clusters with gene(s) from the NRC-

144   S clade, and are widely distributed in Cornales, campanulids and lamiids, but absent in Ericales.

145   We experimentally validated the functional connections between NRC0 and genetically linked

146   NRC-S (NRC0-S) in the *Nicotiana benthamiana* model system. Furthermore, activation of a

147   tomato NRC0-S resulted in high-order complex formation of its genetically linked NRC0

148   similar to the oligomerization observed for other NRCs (Contreras et al., 2023a; Contreras et

149   al. 2023b; Ahn et al., 2023). We propose that the *NRC0* sensor-helper gene cluster reflects the

150   ancestral state of the NRC network; the *NRC0* cluster emerged early in asterid evolution and

151   has massively expanded into immune receptor networks in the Solanaceae and related asterid

152   species. This study highlights contrasting evolutionary dynamics between the functionally

153   conserved *NRC0* gene cluster and the massively expanded and genetically dispersed NRC

154   network of lamiid plants.

155

156   **RESULTS**

157

158   ***NRC0* is the most conserved NRC helper gene in asterids**

159

160   We hypothesized that the most conserved NRC gene across asterid species is most likely to

161   reflect the ancestral state of the expanded NRC networks. To determine the distribution of

162   helper NRC (NRC-H) genes across plant species, we first annotated NLR genes from reference

163   genome databases of six representative plant species from asterids: carrot (*Daucus carota,*

164   DCAR-), monkey flower (*Mimulus guttatus,* Migut-), coffee (*Coffea canephora,* Cc-), wild

165   sweet potato (*Ipomoea trifida,* itf-), *Nicotiana benthamiana* (NbS-) and tomato (*Solanum*

166   *lycopersicum*, Solyc-) by using the NLRtracker pipeline (Kourelis et al., 2021) (Supplemental

167   File 1). To classify NRC superclade genes from the asterid NLRome dataset, we performed a

168   phylogenetic analysis using the NB-ARC domain sequences of 1,661 annotated NLRs and 39

169   functionally validated NLRs (Figure 1A). In total, we identified 83 NRC-H genes from six

170   plant species (one gene from carrot; 11 genes from monkey flower; 13 genes from coffee; 36
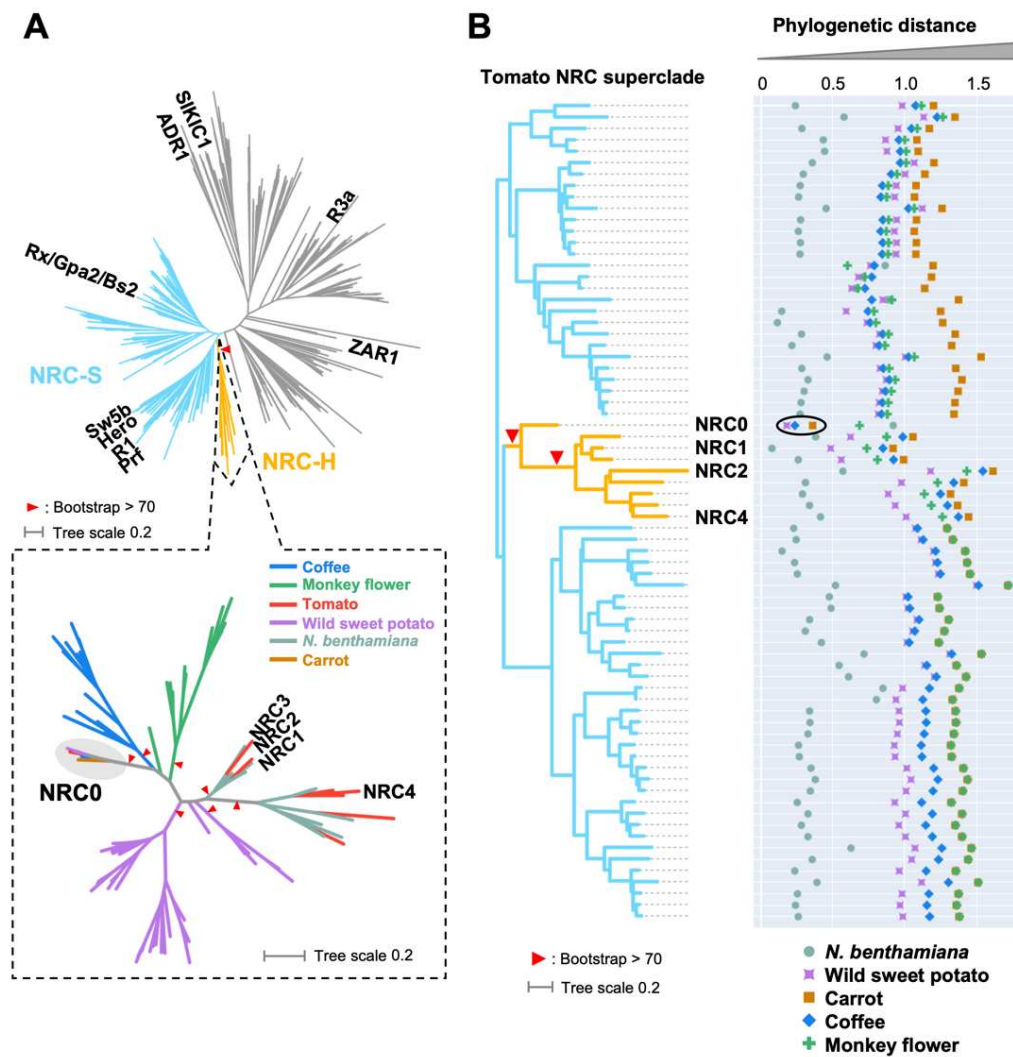
171
172
Figure 1. *NRC0* is the most conserved helper clade NRC in asterids. (A) Phylogeny of NLRs identified from asterids
(carrot, monkey flower, coffee, wild sweet potato, *Nicotiana benthamiana*, and tomato). The maximum likelihood
phylogenetic tree was generated in RAxML version 8.2.12 with JTT model using NB-ARC domain sequences of 1,661 NLRs
identified from carrot, monkey flower, coffee, wild sweet potato, *N. benthamiana*, and tomato reference genome by using the
NLRtracker and 39 functionally validated NLRs. In the top left phylogenetic tree, the NRC superclades are described with
different branch color codes: NRC-helper (NRC-H) subclade shown in orange and NRC-sensor (NRC-S) subclades shown in
light blue. The bottom left phylogenetic tree describes NRC-H subclade with different color codes based on plant species. Red
arrow heads indicate bootstrap support > 0.7 and is shown for the relevant nodes. **(B)** Phylogenetic distance of two NRC-H
and NRC-S nodes between tomato and other plant species. The phylogenetic distance was calculated from the NB-ARC
phylogenetic tree shown in A. The closest distances are plotted with different colors based on plant species. Representative
tomato NRC-H are highlighted.

184

genes from wild sweet potato; 13 genes from *N. benthamiana*; nine genes from tomato)
(Supplemental Figure S1). While most of the NRC-H form plant lineage specific subclades or
clusters with previously defined Solanaceae (*N. benthamiana* and tomato) NRC-H subclade,
there is one unique NRC-H subclade containing NRC-H sequences derived from four different

189   plant species, carrot, coffee, wild sweet potato and tomato (Figure 1A; Supplemental Figure

190   S1). We named the subclade NRC0, with each of the four species having one or two *NRC0*

191   orthologous   genes   (DCAR_023561,   Cc11_g06560,   itf14g00240,   itf14g00270,

192   Solyc10g008220) (Supplemental Table S1). In contrast to the four species, *NRC0* was not

193   found in monkey flower and *N. benthamiana*.

194

195   To further evaluate *NRC0* conservation relative to other NRC-H, we used a phylogenetic tree

196   of 805 NLR genes including NRC-H and NRC-S from the six asterid species (carrot, monkey

197   flower, coffee, wild sweet potato, *N. benthamiana* and tomato) and nine functionally validated

198   NRCs to calculate the phylogenetic (patristic) distance between each of the 72 tomato NRC-

199   H/-S and their closest neighbor gene from each of the other plant species. We found that NRC0

200   displays the shortest patristic distance to its orthologs compared to other NRCs (Figure 1B).

201   These phylogenetic analyses suggest that *NRC0* is possibly the most widely conserved helper

202   NRC-H gene in asterids.

203

204   **Comparative analyses of NLR genes across asterid genomes identify a conserved *NRC0***

205   **gene cluster of candidate sensors and helpers**

206

207   Plant sensor and helper NLRs often function in genetically linked pairs, while solanaceous

208   NRCs such as NRC2, NRC3 and NRC4, form phylogenetically related but genetically

209   dispersed NLR networks (Wu et al., 2017). To determine the degree to which helper NLRs,

210   including *NRC0*, form NLR gene clusters in the genome, we conducted gene cluster analysis

211   of whole NLRomes annotated from four asterid species, carrot, coffee, wild sweet potato, and

212   tomato. In this analysis, we extracted genetically linked NLRs that have genetic distances less

213   than 50 kb. The gene cluster information was mapped onto the NLR phylogenetic tree of the

214   four plant species. In total, we found 1,146 genetically linked gene pairs in NLRomes of the

215   four plant species (141 gene clusters in carrot, 324 gene clusters in coffee, 536 gene clusters in

216   wild sweet potato, 145 gene clusters in tomato) (Supplemental Figure S2; Supplemental Table

217   S2 and Supplemental Data Set 1).

218

219   In the NRC superclade, 438 genetically linked gene pairs exist in the genomes (three gene

220   clusters in carrot, 45 gene clusters in coffee, 347 gene clusters in wild sweet potato, 43 gene

221   clusters in tomato) (Figure 2A; Supplemental Table S2 and Supplemental Data Set 1). Out of

222   438 gene pairs, 378 are NRC-S gene pairs and 47 are NRC-H gene pairs. Notably, there are 13
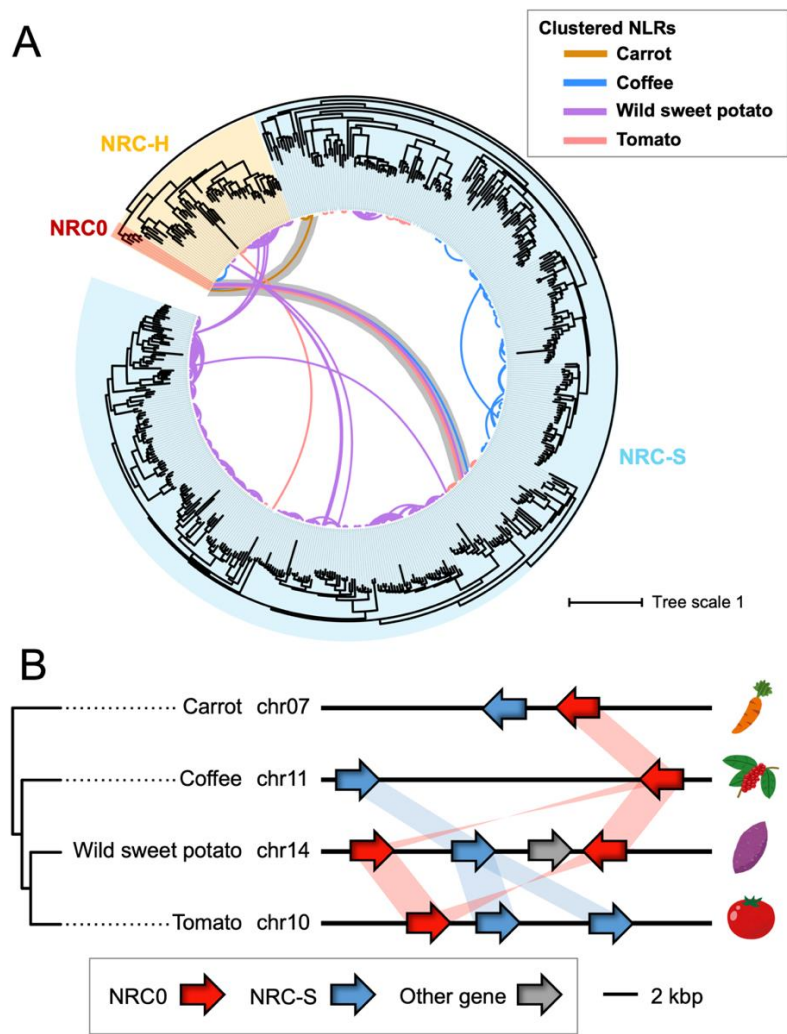
Figure 2. *NRC0* form a conserved gene cluster with members of the NRC sensor clade in asterids. (A) Phylogeny of NRC family genes from carrot, coffee, wild sweet potato and tomato with NLR gene cluster information. The maximum likelihood phylogenetic tree was generated in RAxML version 8.2.12 with JTT model using NB-ARC domain sequences of 513 NRCs identified in Figure 1. The NRC subclades are described with different background colors: NRC0 (red), other NRC-H (yellow), and NRC-S (blue). The connected lines between nodes indicate genetically linked NLRs (distance < 50 kb) with different colors based on plant species. Genetic link between *NRC0* and *NRC-S* are highlighted in gray. (B) Schematic representation of *NRC0* loci in carrot, coffee, wild sweet potato and tomato. Red, blue and gray arrows indicate *NRC0*, *NRC-S* genetically linked with *NRC0*, and other gene, respectively. Red and blue bands indicate phylogenetically related genes.

genetically linked gene pairs that consist of both NRC-H and NRC-S genes (Figure 2A). Among them, only six gene pairs are conserved in the four plant species and are formed by *NRC0* and NRC-S clade genes (DCAR_023560 and DCAR_023561, Cc11_g06550 and Cc11_g06560, itf14g00240 and itf14g00250, itf14g00250 and itf14g00270, Solyc10g008220 and Solyc10g008230, Solyc10g008220 and Solyc10g008240) (Figure 2A, 2B). Although we found seven additional gene clusters (six gene clusters in sweet potato, one gene cluster in tomato), these gene clusters appeared to be plant lineage-specific (Figure 2A; Supplemental

240   Table S2). CC_R-NLRs, ADR1 and NRG1, are also known as conserved helper subfamily genes

241   (Shao et al., 2016; Baggs et al., 2020; Liu et al., 2021). We noted that ADR1 and NRG1 in

242   carrot, coffee, wild sweet potato, and tomato, form gene clusters with their paralogs, but not

243   with genes from other NLR subfamilies (Supplemental Figure S2; Supplemental Table S2 and

244   Supplemental Data Set 1). Taken together, these findings suggest that *NRC0* stands out as a

245   widely conserved gene cluster of candidate helper-sensor NLRs in asterids.

246

247   **The *NRC0* gene cluster predates the NRC expansion in lamiid*s***

248

249   To further examine the distribution of the *NRC0* gene cluster across plant species, we searched

250   for *NRC0* orthologs by running a two-stage computational pipeline based on iterated BLAST

251   searches of plant genome and protein databases and phylogenetic analysis (Figure 3A). First,

252   we defined NRC-H genes as *NRC0* orthologs if the NRC-H genes belong to a phylogenetically

253   well-supported clade with *NRC0* from carrot, coffee, wild sweet potato and tomato (Figure 3A,

254   3B). Based on this definition, we identified 38 *NRC0* orthologs from 26 asterid species, that

255   classified in the NRC0 phylogenetic subclade (Figure 3A, 3B; Supplemental Table S1). In the

256   second stage, we applied gene cluster analysis to identify NLR genes which are genetically

257   linked to the obtained *NRC0* orthologs (Figure 3A). Among the 38 *NRC0* ortholog genes, 20

258   *NRC0* genes from 17 species are genetically linked with 23 NLR genes in NRC-S subclades

259   (Figure 3A, 3B).

260

261   Based on our criteria for the *NRC0* phylogenetic and genetic cluster, *NRC0* orthologs and their

262   genetically linked NLRs (referred to as NRC0-dependent sensor candidates: NRC0-S) are

263   widely distributed in asterids, Cornales, campanulids, and lamiids, but absent in Ericales

264   (Figure 4A; Supplemental Table S1). Overall, these results suggest that the *NRC0* gene cluster

265   emerged early in the asterid lineage.

266

267   In addition to the gene distribution analysis of *NRC0*, we investigated the number of other

268   NRC-H and NRC-S genes across asterid species. We used NLRtracker to annotate NLR genes

269   from 31 asterid species and one Caryophyllales species, and classified NRC-H and NRC-S

270   genes based on phylogenetic analysis. We found NRC-H and NRC-S are drastically expanded

271   in lamiids, compared to other plant orders in asterids (Figure 4B; Supplemental Table S3 and

272   Supplemental File 12). In Cornales, Ericales, and campanulids, the number of NRC-H genes

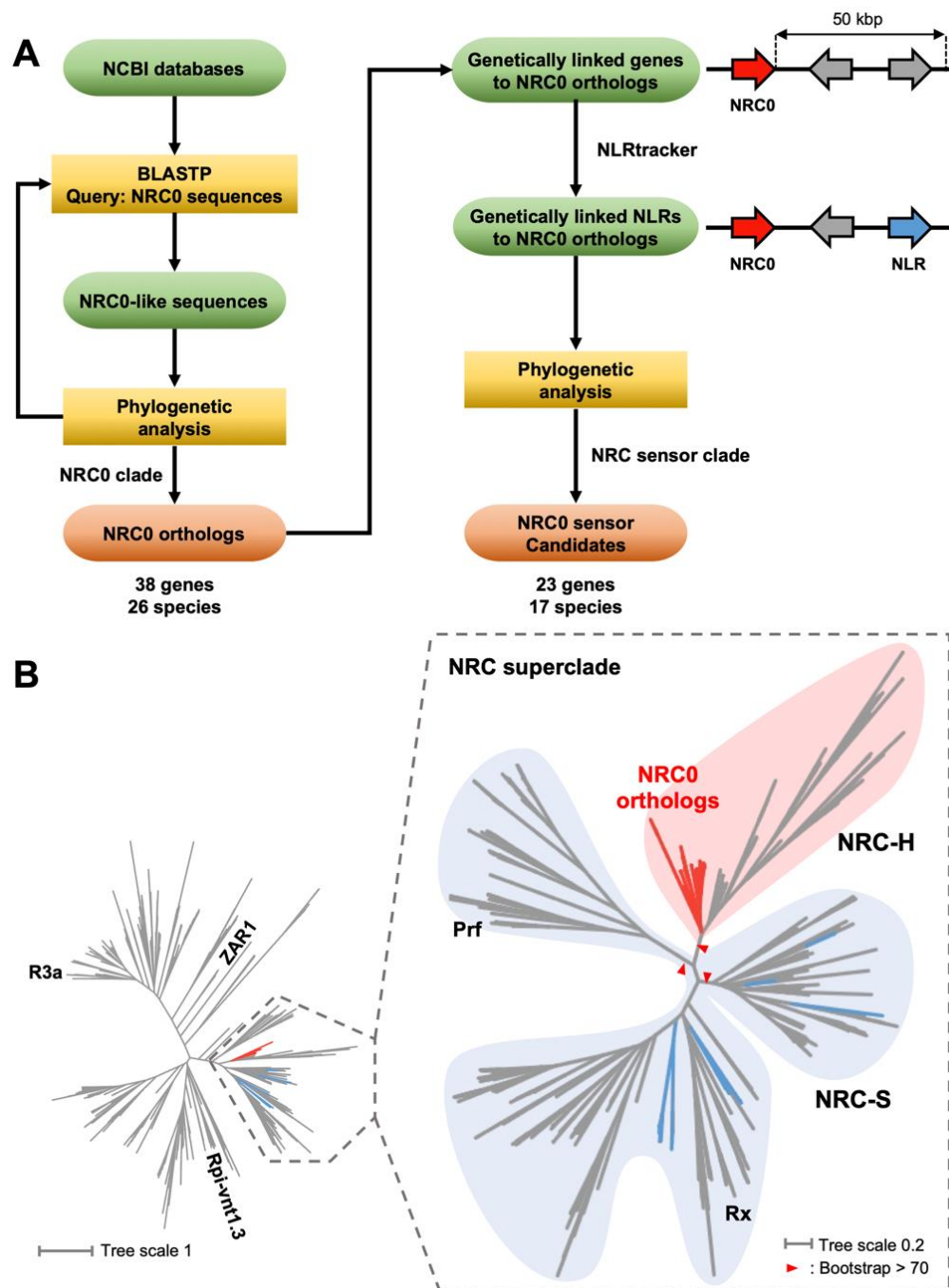273   range from 1 to 8 and that of NRC-S genes range from 0 to 31 across species (Figure 4B;

Figure 3. Phylogenomic analyses identify 38 *NRC0* orthologs from 26 asterid species that are linked to 23 *NRC0-S* in 17 species. (A) Workflow for computational analyses in searching *NRC0* orthologs and *NRC0-S* candidates. TBLASTN/BLASTP searches and subsequent phylogenetic analyses were performed to identify *NRC0* orthologs from plant genome/proteome datasets. We extracted *NRC0-S* candidates by performing gene cluster, the NLRtracker (Kourelis et al., 2021) and phylogenetic analyses. **(B)** *NRC0* orthologs exist in a subclade of the NRC-H clade. The maximum likelihood phylogenetic tree was generated in RAxML version 8.2.12 with JTT model using NB-ARC domain sequences of NRC0, NRC0-S, 15 functionally validated CC-NLRs and 1,194 CC-NLRs identified from six representative asterids, *Nyssa sinensis*, *Camellia sinensis*, *Cynara cardunculus*, *Daucus carota*, *Sesamum indicum* and *Solanum lycopersicum*. Red and blue branches indicate NRC0 and NRC0-S, respectively. Red arrow heads indicate bootstrap support > 0.7 and is shown for the relevant nodes.
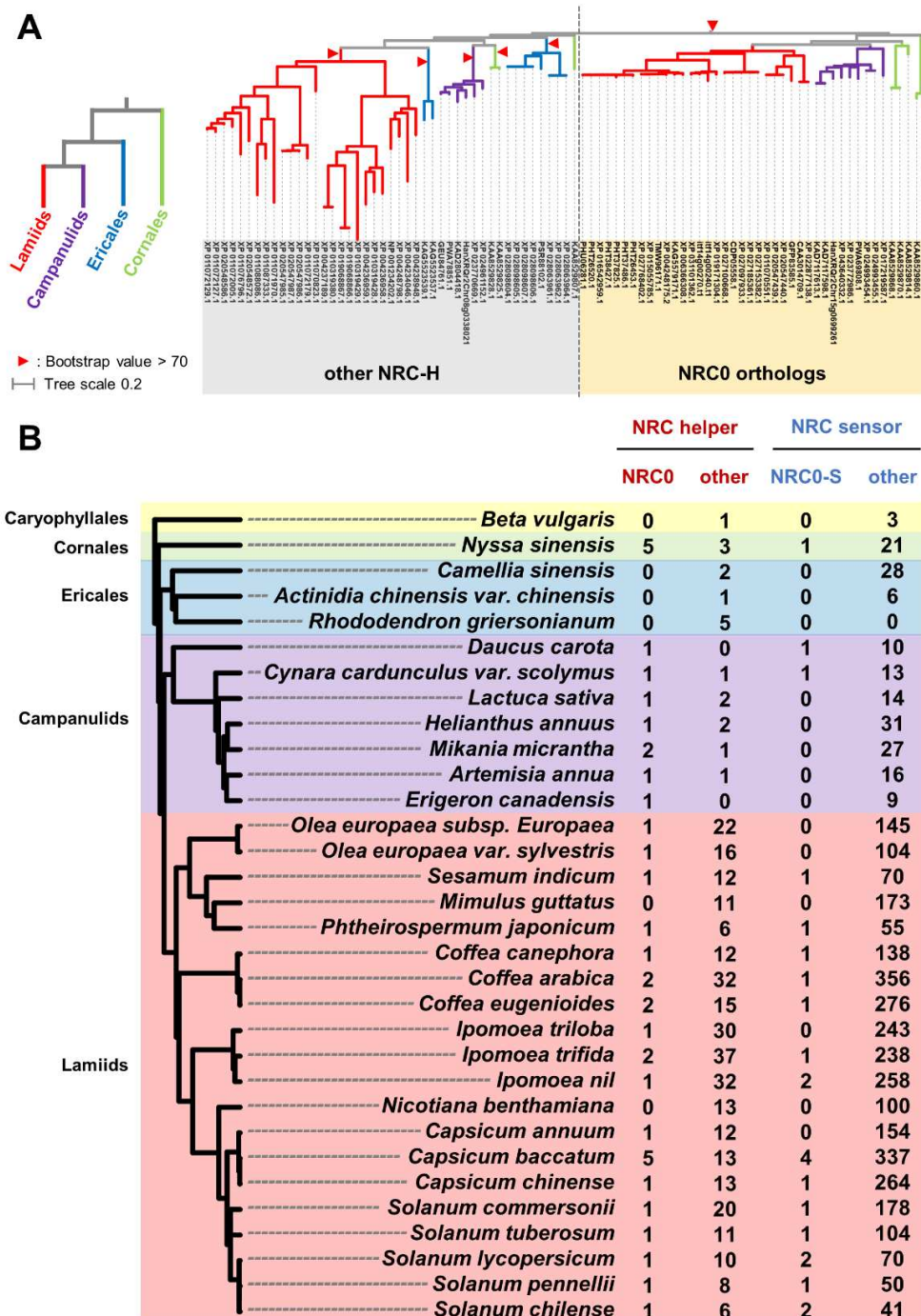
Figure 4. The *NRC0* gene cluster predates the massively expanded NRC network of lamiids. **(A)** Phylogeny of NRC helper subfamily defines *NRC0* orthologs and other NRCs. The maximum likelihood phylogenetic tree was generated in RAxML version 8.2.12 with JTT model using full length amino acid sequences of 87 NRC-H. The phylogenetically well-supported clade (bootstrap value > 70) containing NRC0 from Cornales, campanulids and lamiids are defined as the NRC0 subclade. The plant orders are described with different branch colors. **(B)** Distribution of the number of *NRC* genes across asterids. The left phylogenetic tree of plant species was extracted from a previous study (Smith and Brown, 2018). The right table indicates the number of *NRC0*, other *NRC-H*, *NRC0-S* and other *NRC-S* genes from 31 asterids and one Caryophyllales species. Background colors indicate plant orders.

296   Supplemental Table S3 and Supplemental File 12). In lamiids, the number of NRC-H and

297   NRC-S genes range from 7 to 39 and from 43 to 357, respectively (Figure 4B; Supplemental

298   Table S3 and Supplemental File 12). Taken together, the expansion of NRC genes occurred

299   primarily in lamiids species, but not in other asterid plants.

300

301   **_NRC0_ orthologs carry the N-terminal sequence pattern required for cell death response**

302

303   In the Solanaceae NRC network, the MADA motif remains at the very N terminus of NRC-H,

304   whereas NRC-S have distinct sequences at their N-terminal region (Adachi et al., 2019a).

305   Therefore, we hypothesized that NRC0 orthologs carry the MADA motif at their N termini for

306   induction of cell death responses. To test this, we first ran MEME (Multiple EM for Motif

307   Elicitation; Bailey and Elkan 1994) to search for conserved sequence patterns among the 38

308   NRC0 orthologs and 23 NRC0-S, respectively. All NRC0 and 10 NRC0-S carry typical CC-

309   NB-LRR domain architecture, while 13 NRC0-S lack either CC or LRR domains

310   (Supplemental Table S1). None of the NRC0 or NRC0-S were annotated with integrated

311   domains that can be found in sensor NLRs for effector recognition (Figure 5; Supplemental

312   Table S1). MEME analysis revealed 20 conserved sequence motifs that span across the NRC0

313   orthologs and 20 conserved sequence motifs that span across NRC0-S (Figure 5; Supplemental

314   Table S4 and S5). Within the MEME motifs, 2nd and 9th MEME in the NB-ARC domain of

315   NRC0 and 2nd and 8th MEME in the NB-ARC domain of NRC0-S match to p-loop and MHD

316   motifs that coordinate binding and hydrolysis of ATP (Figure 5). Notably, in NRC0 and NRC0-

317   S, we detected a MEME motif that is positioned at the very N-terminus where the MADA motif

318   is generally found (Figure 5). Next, we used the HMMER software (Eddy 1998) to query the

319   NRC0 orthologs and NRC0-S with a previously developed MADA motif–hidden Markov

320   model (MADA-HMM; Adachi et al. 2019a). This HMMER search detected the MADA motif

321   in 89.5% (34/38) of NRC0 orthologs, but in none of the NRC0-S (0/23) (Supplemental Table

322   S1). Indeed, the sequence patterns of the N-termini are different between NRC0 and NRC0-S.

323   Instead of the MADA sequence, NRC0-S have "MAHAAVVSLxQKLxx" sequence at their

324   N-termini (Figure 5).

325

326   To further investigate sequence conservation and variation among NRC0 and NRC0-S, we

327   used ConSurf (Ashkenazy et al., 2016) to calculate a conservation score for each amino acid

328   and generate a diversity barcode for NRC0 and NRC0-S, respectively (Figure 5). NRC0

329   orthologs have highly conserved amino acid sequences across their entire domains and display
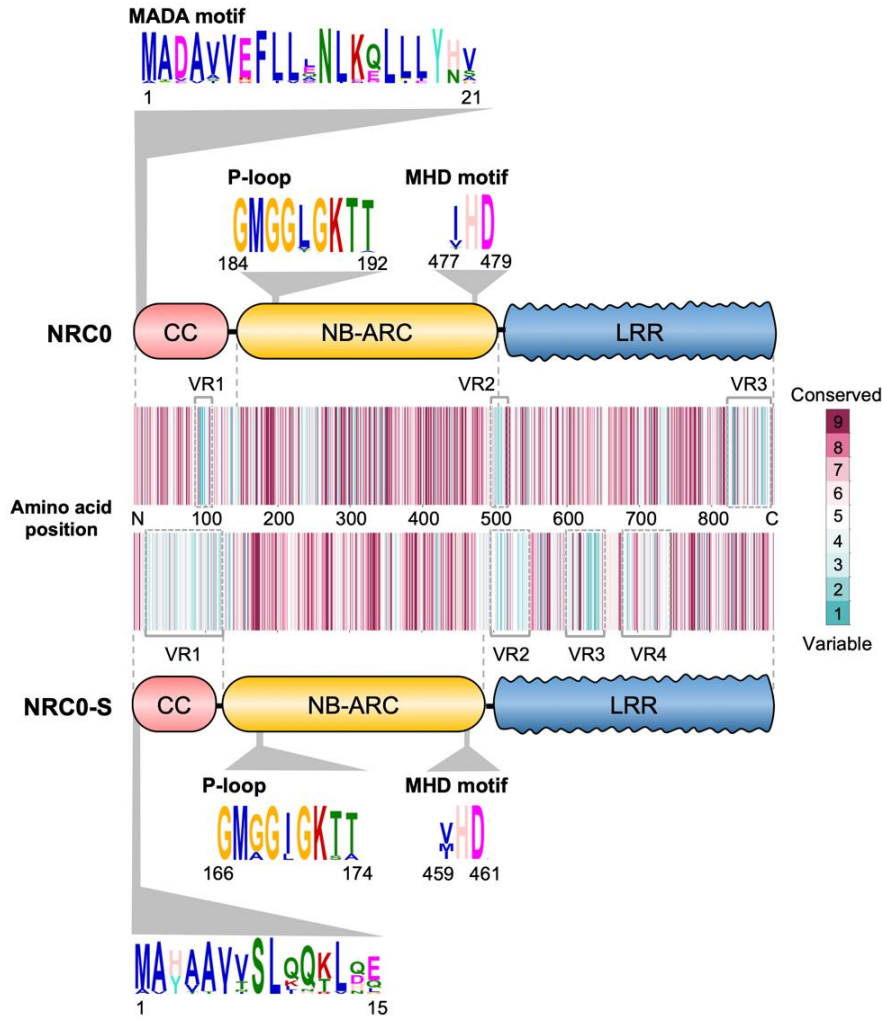
330
331 **Figure 5. NRC0 orthologs, but not their genetically linked sensors, carry the N-terminal MADA motif required for**
332 **hypersensitive cell death response.** Schematic representation of conserved sequence patterns across NRC0 orthologs and
333 NRC0 sensor candidates (NRC0-S). Consensus sequence patterns were identified by MEME using amino acid sequences of
334 38 NRC0 orthologs and 23 NRC0-S, respectively. Conservation and variation of each amino acid among NRC0 orthologs and
335 NRC0-S were calculated on amino acid alignment via the ConSurf server (https://consurf.tau.ac.il). The conservation scores
336 are mapped onto each amino acid position in tomato NRC0 (XP_004248175.2) and tomato NRC0-S (XP_004248174.1).

337

338 few variable regions (VR) at the middle of CC domain (VR1), junction of NB-ARC and LRR
339 domains (VR2) and C-terminal end of LRR domain (VR3) (Figure 5). In the case of NRC0-S,
340 the amino acid sequence is varied in the CC and LRR domains (VR1 ~ V4), although the NB-
341 ARC domain sequence is highly conserved across NRC0-S (Figure 5).

342

343 Taken together, NRC0 orthologs carry highly conserved sequences throughout the full protein
344 and display a canonical N-terminal MADA motif. In contrast, NRC0-S tend to be more variable
345 especially in the CC and in parts of the LRR domains and lack a typical MADA motif.

346

NRC0 are helper NLRs functionally connected with their genetically linked NLR sensors

Since NRC0, but not NRC0-S, carry the MADA motif at their N-termini, we hypothesized that NRC0 functions as a helper and NRC0-S relies on its genetic partner NRC0 to trigger immune responses. To experimentally validate this hypothesis, we first cloned *NRC0* and *NRC0-S* genes from carrot (DcNRC0: DCAR_023561, DcNRC0-S: DCAR_023560) , coffee (CcNRC0: Cc11_g06560, CaNRC0-S: XM_027242939.1 in *Coffea arabica*, orthologous gene to Cc11_g06550), wild sweet potato (ItNRC0a: itf14g00240, ItNRC0b: itf14g00270, ItNRC0-S: itf14g00250) and tomato (SlNRC0: Solyc10g008220, SlNRC0-Sa: Solyc10g008230, SlNRC0-Sb: Solyc10g008240) as wild-type sequences (referred to as NRC0^{WT} or NRC0-S^{WT}) (Figure 6A). We introduced an aspartic acid (D) to valine (V) mutation in the MHD motif to generate autoactive mutants of each NLR (referred to as NRC0^{DV} or NRC0-S^{DV}) and tested the autoactive cell death activity in *Nicotiana benthamiana,* a species that does not have NRC0 in its genome (Figure 4B). Interestingly, four out of five tested NRC0, DcNRC0, CcNRC0, ItNRC0b and SlNRC0 caused macroscopic cell death in *N. benthamiana* leaves when expressed as MHD mutants, but the NRC0-S did not (Figure 6B, 6C). As a control, we expressed the *N. benthamiana* NRC-H NRC4 MHD mutant which causes autoactive cell death (Adachi et al., 2019a) (Figure 6B, 6C). Although we occasionally observed weak cell death by expressing DcNRC0-S^{DV} and SlNRC0-Sb^{DV}, there was no visible cell death when expressing the majority of the DcNRC0-S^{DV} and SlNRC0-Sb^{DV} constructs, similar to the other NRC0-S (Figure 6B, 6C). This result suggests that the MADA-type CC-NLR NRC0, but not NRC0-S, has the capacity to trigger hypersensitive cell death by itself.

Our observation that *NRC0-S* are genetically clustered with helper *NRC0* prompted us to determine whether NRC0-S functionally connects with NRC0. To test this, we expressed NRC0-S MHD mutants with or without their genetically linked wild-type NRC0 in the *nrc2/3/4* knockout *N. benthamiana* line. Notably, we observed that some NRC0-S MHD mutants showed macroscopic cell death in the presence of their genetically linked NRC0 (Figure 6D, 6E). For instance, co-expression of DcNRC0-S^{DV} and DcNRC0^{WT}, CaNRC0-S^{DV} and CcNRC0^{WT}, ItNRC0-S^{DV} and ItNRC0b^{WT}, SlNRC0-Sa^{DV} and SlNRC0^{WT} triggered a cell death response (Figure 6D, 6E). In this experiment, Rx was used as a control of NRC-dependent sensor NLR functioning with NRC-H NRC2, NRC3 and NRC4 (Wu et al., 2019). NRC4 expression complemented cell death response triggered by an autoactive MHD mutant of Rx
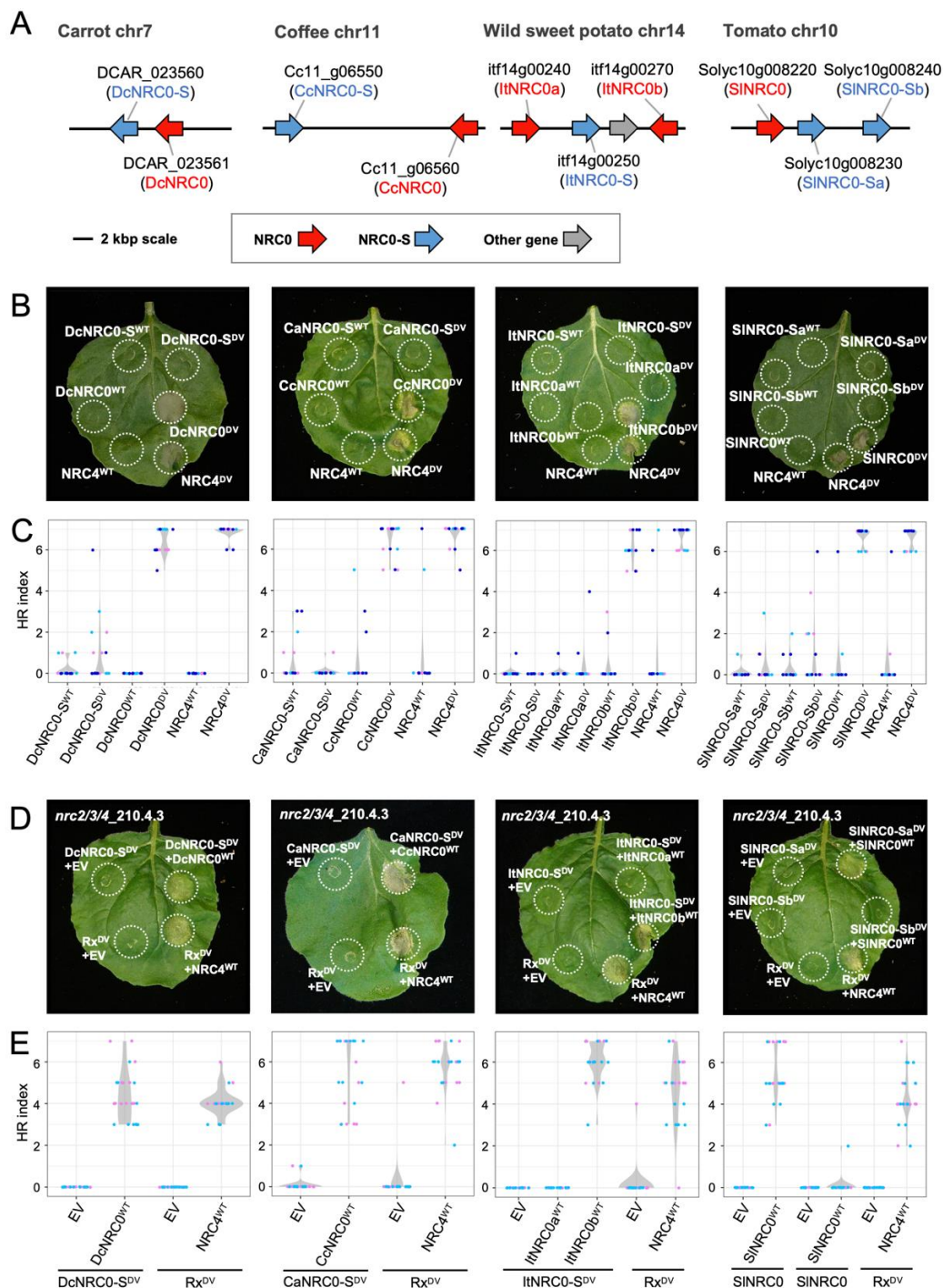
Figure 6. NRC0 is required for the genetically linked NRC sensor to trigger the hypersensitive cell death response in *Nicotiana benthamiana*. (**A**) Schematic representation of *NRC0* loci in carrot, coffee, wild sweet potato, and tomato. Red and blue arrows indicate *NRC0* and *NRC0-S*, respectively. Gray arrow indicates other gene. (**B**) Wild-type NRC0, NRC0-S, NRC4 and the MHD mutants were expressed in *N. benthamiana* leaves by agroinfiltration. Cell death phenotype was recorded five days after the agroinfiltration. (**C**) Violin plots showing cell death intensity scored as an HR index based on three independent experiments of B. (**D**) Representative images of autoactive cell death after co-expression of wild-type NRC0 (NRC0^{WT}) and MHD mutants of NRC0 sensor (NRC0-S^{DV}) in *N. benthamiana nrc234* mutant line. Empty vector (EV), wild-type NRC4 (NRC4^{WT}) and the MHD mutant of sensor Rx (Rx^{DV}) were used as controls. Photographs were taken at five days after agroinfiltration. (**E**) Violin plots showing cell death intensity scored as an HR index based on two independent experiments of D.

392 (Rx^{D460V}; Bendahmane et al., 2002) in the *nrc2/3/4* knockout line (Figure 6D, 6E). Our results

393 indicate that NRC0-S require the genetically linked NRC0 to trigger immune response.

394

Co-expression of mis-matched NRC0 and NRC0-dependent sensor pairs from different asterid species reveals evolutionary divergence

397

398 Our finding that the *NRC0* cluster is conserved in asterid species suggested that NRC0 and

399 NRC0-S are functionally paired across asterids. However, the degree to which co-evolution

400 between sensors and helpers has resulted in functional incompatibilities over evolutionary time

401 is unclear. We explored whether sensor-helper pairs have functionally diverged over

402 evolutionary time by co-expressing mis-matched pairs from different species, i.e. MHD

403 mutants of each NRC0-S with wild-type NRC0 from four asterid species (carrot, coffee, wild

404 sweet potato, and tomato) in the *nrc2/3/4 N. benthamiana* mutant line. We observed functional

405 connections between NRC0-S and NRC0 across asterids with different specificities (Figure 7A,

406 7B; Supplemental Figure S3). For instance, co-expression of either DcNRC0-S^{DV} or CaNRC0-

407 S^{DV} and four tested NRC0, DcNRC0^{WT}, CcNRC0^{WT}, ItNRC0b^{WT} or SlNRC0^{WT}, triggered cell

408 death response (Figure 7A, 7B; Supplemental Figure S3). Unlike carrot and coffee NRC0-S,

409 ItNRC0-S^{DV} and SlNRC0-Sa^{DV} triggered cell death response only with ItNRC0b^{WT} or

410 SlNRC0^{WT} (Figure 7A, 7B; Supplemental Figure S3). As a control, we co-expressed NRC4^{WT}

411 with DcNRC0-S^{DV}, CaNRC0-S^{DV}, ItNRC0-S^{DV} and SlNRC0-Sa^{DV} and 67~84% of tested

412 samples did not show macroscopic cell death response (Figure 7A, 7B; Supplemental Figure

413 S3). Taken together, NRC0-S in carrot, a species of campanulids, and coffee, the early

414 divergent lamiids, showed functional connections across all of the tested NRC0, while NRC0-

415 S in wild sweet potato and tomato were specifically functional only with NRC0 from Solanales.

416

Activated NRC0-dependent sensor leads to high-order complex formation of its genetically linked helper NRC0

419

420 Given that activation of NRC-dependent sensors induces homo-oligomerization of helper

421 NRCs in the genetically dispersed NRC network (Contreras et al., 2023a; Ahn et al., 2023), we

422 hypothesized that activation of NRC0-S leads to oligomerization of its genetic partner NRC0.

423 To test this hypothesis, we first generated a MADA motif mutant of tomato NRC0

424 (SlNRC0$^{L9E/L13E/L17E}$, referred to as SlNRC0^{EEE}) (Figure 8A). This mutation suppresses cell

425 death induction by MADA-type NLRs without inhibiting their resistosome formation (Adachi
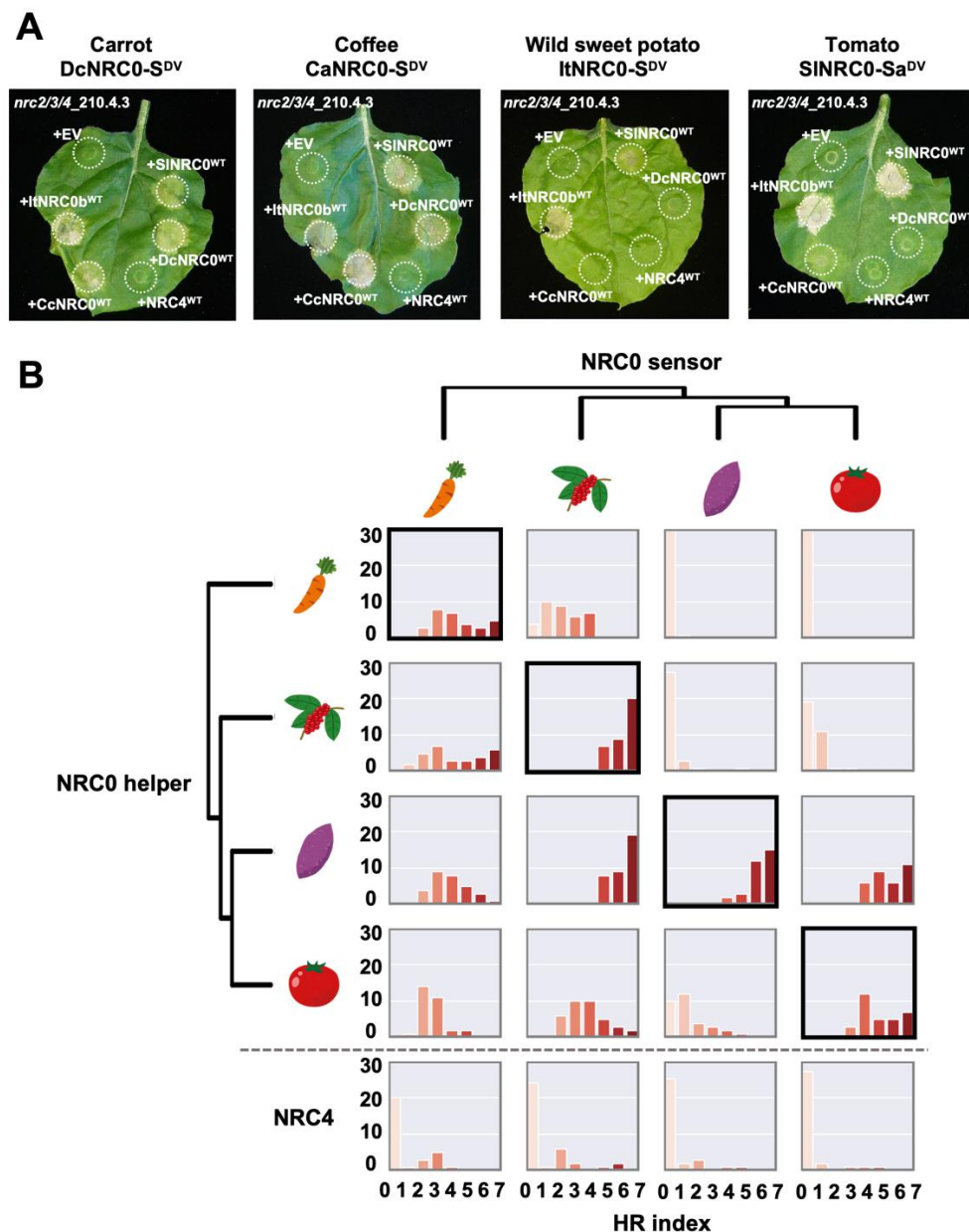
Figure 7. NRC0 sensors have different compatibility in inducing the hypersensitive cell death with NRC0 orthologs from across asterids. (A) Photographs show representative images of autoactive cell death after co-expression of MHD mutants of NRC0 sensor (NRC0-S^{DV}) with wild-type NRC0 (NRC0^{WT}) from four asterid species (carrot, coffee, wild sweet potato and tomato) in *N. benthamiana nrc2/3/4* mutant line. Empty vector (EV) and wild-type NRC4 (NRC4^{WT}) were used as controls. Photographs were taken at five days after agroinfiltration. (B) Matrix showing the cell death response triggered by NRC0 and NRC0-S^{DV}. Histograms describe cell death intensity scored in Supplemental Figure S3.

et al., 2019a; Hu et al., 2020; Förderer et al., 2022; Contreras et al., 2023a; Ahn et al., 2023). We expressed SlNRC0^{EEE} in *nrc2/3/4* knockout *N. benthamiana* lines with wild-type SlNRC0-Sa or its autoactive mutant SlNRC0-Sa^{DV} (Figure 8A). In inactive state with wild-type SlNRC0-Sa, SlNRC0^{EEE} was detected as a smear migrating mostly below ~480 kDa in BN-PAGE assay (Figure 8B). Upon activation by co-expressing SlNRC0-Sa^{DV}, SlNRC0^{EEE} shifted
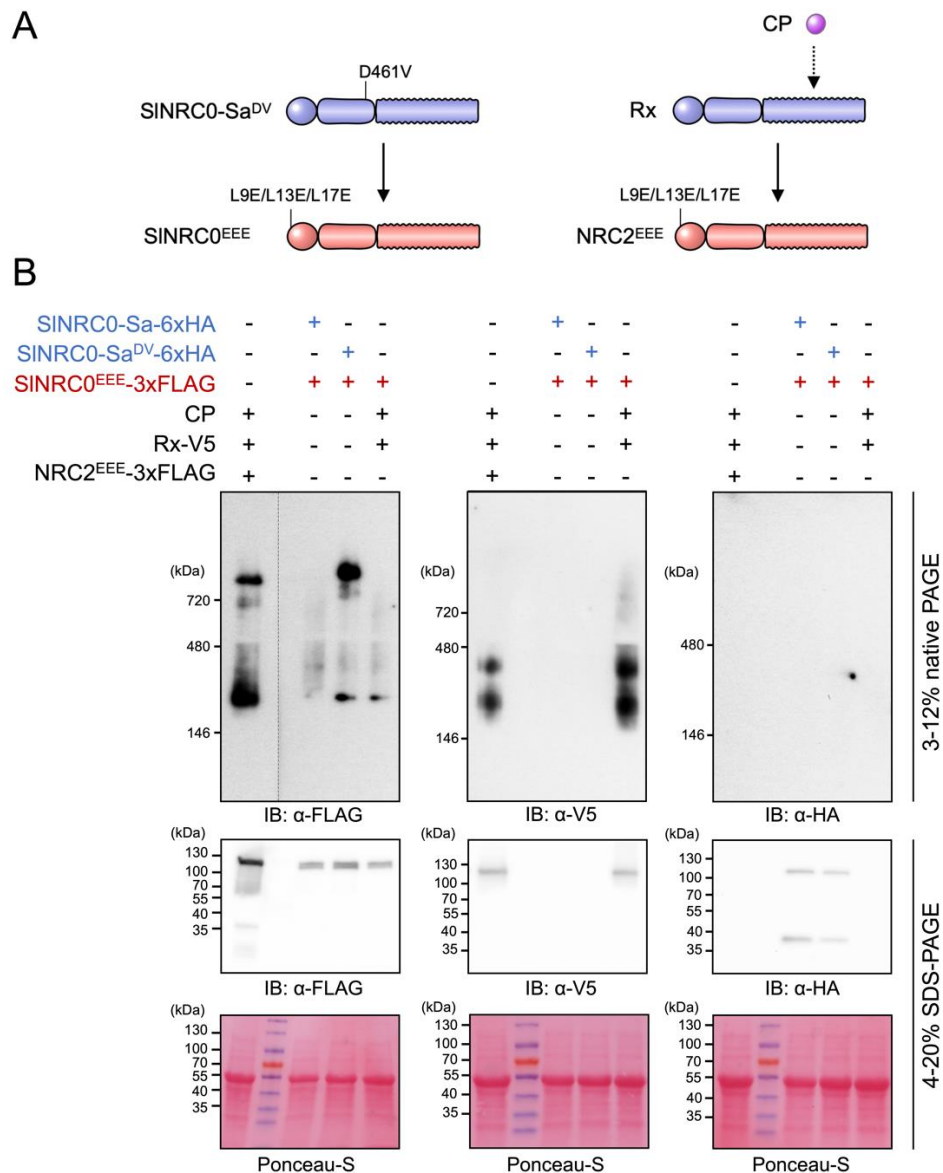
Figure 8. An autoactive NRC0-dependent sensor leads to formation of an NRC0 higher-order complex in *Nicotiana benthamiana*. (A) Schematic representation of helper NRC activation by sensor NLRs. (B) Detection of activated NRC0 complex in BN-PAGE. Each *Agrobacterium* strain carrying wild-type SlNRC0 sensor (SlNRC0-Sa), SlNRC0-Sa MHD mutant (SlNRC0-Sa^{DV}), MADA motif mutant of SlNRC0 (SlNRC0^{EEE}), *Potato virus X* coat protein (CP), wild-type Rx (Rx) or MADA motif mutant of NRC2 (NRC2^{EEE}) was inoculated to leaves of an *N. benthamiana nrc2/3/4* mutant line. Total proteins were extracted from the inoculated leaves at three days after agroinfiltration. Extracts were run in native and SDS-PAGE gels, and immunoblotted with anti-FLAG, anti-V5 and anti-HA antibodies, respectively. Loading control was visualized with Ponceau-S staining. The higher-order complex of activated NRC0 was detected in three independent experiments.

to slow-migrating higher molecular weight complex visible as a band above the 720 kDa marker (Figure 8B). This higher-order complex band of SlNRC0^{EEE} was not observed in a sample co-expressing Rx and its cognate ligand *Potato virus X* coat protein (CP), while activated Rx and CP co-expression induced oligomerization of NRC2^{EEE} in the control

454   treatment (Contreras et al., 2023a) (Figure 8B). In this BN-PAGE assay, activated SlNRC0

455   showed relatively slower migration than the NRC2 oligomer (Figure 8B). This result suggests

456   that like other NRC helpers, activated NRC0 may form the ZAR1 resistosome-type high-order

457   complex.

458

459   Contreras et al. (2023a) and Ahn et al. (2023) showed NRC-dependent sensor NLRs are not

460   present in the high-order complex of activated NRC, thereby proposing a model that the NRC

461   resistosome is a homo-oligomeric complex. To investigate whether NRC0-dependent sensor

462   NLR is associated with the activated NRC0 complex, we immunoblotted SlNRC0-Sa in the

463   BN-PAGE assay. Although protein accumulation of wild-type SlNRC0-Sa and SlNRC0-Sa^{DV}

464   were confirmed in an immunoblot of the SDS-PAGE assay, both signals were not detected in

465   the BN-PAGE assay immunoblotted by anti-HA antibody (Figure 8B). In the control

466   experiment, activated Rx appeared with two bands in the range of 146 to 480 kDa, as reported

467   previously (Contreras et al. 2023a) (Figure 8B). In this study, we couldn't unambiguously

468   determine whether activated NRC0-dependent sensor integrates the resistosome complex

469   together with its helper NRC0.

470

471   **DISCUSSION**

472

473   NRC-H and NRC-S are phylogenetically related CC-NLRs that form a major superclade in

474   asterid plants that originated from a common ancestor that predates the split between asterids

475   and Caryophyllales (Wu et al., 2017). In solanaceous plants, the monophyletic NRC proteins

476   function as helper NLRs for multiple sensor NLRs in a sister clade and for cell-surface

477   localized immune receptors (Wu et al., 2017; Kourelis et al., 2022; Zhang et al., 2023). In this

478   study, we investigated the evolutionary and functional dynamics of NRC0, an atypical member

479   of the NRC family. *NRC0* is the only NRC family member that is conserved across asterid

480   plants with orthologs in 26 species. *NRC0* orthologs are genetically linked to NRC-S subclade

481   genes. We experimentally validated the functional connections within *NRC0* gene clusters for

482   four distantly related asterid species and revealed that *NRC0* is essential for the hypersensitive

483   cell death response triggered by its genetically linked partner *NRC0-S*. Furthermore, activated

484   NRC0-S leads to the formation of an NRC0 high molecular weight complex similar to the

485   model reported for other NRC-S/NRC-H pairings. We propose that the *NRC0* sensor/helper

486   gene cluster reflects an ancestral state that predates the massive expansion of the NRC network

487   in the lamiid lineage of asterid plants. Our findings fill a gap in the evolutionary history of an

488   NLR network in plants and illustrates contrasting patterns of macroevolution within this

489   complex NLR network (Figure 9).

490

491   The *NRC0* gene cluster most likely emerged early in asterid evolution, which corresponds to

492   about 125 mya based on the dating analyses of Wikström et al. (2015) (Figure 9). A previous

493   phylogenomic study proposed that the NRC superclade expanded from a genetically linked

494   NLR pair over 100 mya before asterids and Caryophyllales lineages split, because an NRC

495   gene cluster exists in Caryophyllales *Beta vulgaris* (sugar beet) (Wu et al., 2017). Consistent

496   with this, we identified one NRC-H and three NRC-S genes from *B. vulgaris*. However, the

497   sugar beet NRC-H gene doesn't map to the NRC0 subclade (Figure 4B). Therefore, the *NRC0*

498   gene cluster probably originated from a common ancestral NLR pair that might be shared with

499   the Caryophyllales NRC gene pair. We hypothesize that later during asterid evolution, the

500   *NRC0* gene pair or a paralogous NLR gene pair have duplicated and expanded into complex

501   NRC networks across asterid genomes (Figure 9). We noted that the expansion and

502   diversification of NRC networks are significant in lamiids. In sharp contrast, Cornales, Ericales

503   and campanulids have experienced limited expansions of NRC-H and NRC-S genes possibly

504   due to low levels of NRC gene duplications and frequent deletions.

505

506   The *NRC0* gene cluster is missing in the Ericales *Camellia sinensis*, *Actinidia chinensis* var.

507   chinensis, and *Rhododendron griersonianum*, and in some other asterid species, such as

508   *Mimulus guttatus* and *Nicotiana benthamiana* (Figure 4B). NLRs are known to be costly genes

509   to plants due to trade-offs between plant growth and NLR-mediated immunity and because

510   they can cause severe autoimmune phenotypes triggered by NLR mis-regulation (Karasov et

511   al., 2017; Adachi et al., 2019b). Thus, the *NRC0* gene cluster may have been lost as a

512   consequence of selection against potential autoimmunity. Notably, five campanulids (*Lactuca*

513   *sativa*, *Helianthus annuus*, *Mikania micrantha*, *Artemisia annua* and *Erigeron canadensis*) and

514   four lamiids (*Olea europaea* subsp. *Europaea*, *Olea europaea* var. *sylvestris*, *Ipomoea triloba*

515   and *Capsicum annuum*) have *NRC0* orthologs but no genetically linked *NRC0-S* encoded

516   within 50 kb genetic distance. It is possible that *NRC0* and *NRC0-S* genes have been genetically

517   dispersed in their genomes like in other sections of the NRC network.

518

519   Both NRC0 and NRC0-S across asterids have a typical CC-NB-LRR domain architecture. In

520   the case of well-studied NLR pairs, Arabidopsis RRS1/RPS4, rice RGA5/RGA4 and Pik-1/Pik-

521   2, the sensor NLRs acquired additional integrated domains that function as decoys to bait
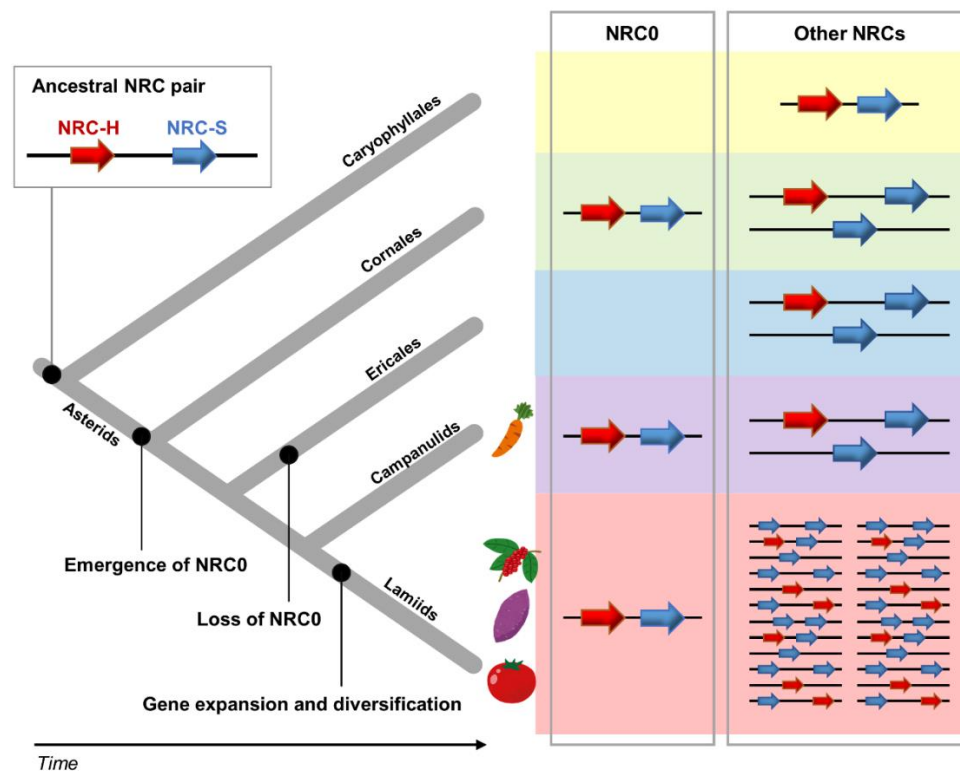
Figure 9. Contrasting patterns of macroevolution in the NRC network of sensor and helper NLRs. The model maps out the key evolutionary transitions in the evolution of the NRC-H and NRC-S throughout 125 million years of evolution. The NLR gene cluster of *NRC0* and *NRC0-S* has presumably originated from an ancestral NRC gene pair, which emerged before Caryophyllales and asterid lineage split. It is likely that the *NRC0* gene cluster has lost in Ericales lineage during asterid evolution. The NRC helper and sensor genes have expanded and genetically dispersed in lamiids species, while NRC components faced limited expansion in Cornales, Ericales and campanulids.

pathogen effectors (Sarris et al., 2015; Le Roux et al., 2015; Césari et al., 2014; Maqbool et al., 2015; Shimizu et al., 2022; Sugihara et al., 2023). Furthermore, in the Solanaceae NRC networks, about half of the NRC-S subclade members acquired N-terminal domain extensions that are often involved in effector recognition (Saur et al., 2015; Li et al., 2019; Adachi et al., 2019; Seong et al., 2020). Since NRC0-S do not have additional predicted domains, NRC-S likely recognize pathogen effectors through their LRR domain as is the case for the ZAR1 and Sr35 CC-NLRs (Wang et al., 2019a; Wang et al., 2019b; Förderer et al., 2022). In terms of effector perception, it is intriguing that the *NRC0* gene cluster is conserved across asterid species over 100 mya. In particular, NLRs are known to exhibit rapid evolution through a birth-and-death model (Michelmore and Meyers 1998). NRC0-S might recognize pathogen effectors in an indirect manner, either monitoring key immune signaling components of the host or functioning with other decoy components.

543 Our sequence motif analysis revealed that NRC0 orthologs have the MADA motif at their N-
544 termini, but their genetically linked NRC0-S partners do not carry the canonical MADA-type
545 sequences of CC-NLRs (Figure 5). This pattern supports the 'use-it-or-lose-it' model in which
546 sensor NLRs lose the molecular signatures of the MADA motif over evolutionary time and
547 instead rely on MADA-type helper NLRs for activation of downstream immune responses
548 (Adachi et al., 2019a). We experimentally demonstrated that NRC0 orthologs can induce the
549 hypersensitive cell death and are required for NRC0-S autoactive cell death (Figure 6).
550 Although NRC0-S are not predicted to have the MADA motif and did not induce cell death
551 without an NRC-0 helper, the "MAHAAVVSLxQKLxx" sequence is conserved at their N
552 termini across NRC0-S proteins (Figure 5). This conservation pattern is striking because other
553 CC domain sequences have been highly diversified among the NRC0-S (Figure 5). The N-
554 terminal MAHA-type sequence may have a role in the molecular function of NRC0-S and was
555 therefore maintained at their N-termini for over 100 million years.

556

557 Our BN-PAGE assays revealed that activated NRC0-S induces the formation of NRC0 high-
558 order complexes (Figure 8). This is consistent with previous findings that activated NRC-S
559 proteins induce formation of homo-oligomerized NRC2 resistosome (Contreras et al., 2023a;
560 Ahn et al., 2023). In this study, we couldn't ascertain whether activated NRC0 forms a
561 resistosome-like high-order complex on its own or together with its sensor partner. This was
562 presumably due to protein stability issues with SlNRC0-Sa under the BN-PAGE conditions
563 (Figure 8). Although further biochemical studies are needed for further mechanistic insight into
564 NRC0 activation, the current results are consistent with the activation-and-release model
565 proposed by Contreras et al. (2023a). In the future, the NRC0 helper-sensor pairs will help map
566 out the evolution of biochemical activation in the NRC network throughout asterid evolution.

567

568 In summary, our study helped reveal an ancestral state of the NRC network resulting in an
569 evolutionary model in which the massively expanded NRC networks evolved from a
570 genetically linked NLR gene pair. As illustrated in Figure 9, the NRC-type NLRs have
571 experienced contrasting patterns of macroevolutionary dynamics over the last 125 million
572 years from a functionally conserved NLR gene cluster to a massive genetically dispersed
573 network. In Solanaceae, the NRC network evolved over tens of millions of years to confer
574 resistance to pathogens and pests as diverse as viruses, bacteria, oomycetes, nematodes and
575 insects. However, the type of pathogen effectors that are recognized by *NRC0* cluster sensor-
576 helper pairs remains unknown. Furthermore, the structure of paired or networked NLR proteins

577 and the determinant of functional specificities between the sensor-helper NLRs are important

578 unanswered questions in the plant NLR research field. The NRC0 pairs will also help to map

579 out the evolution of activation mechanisms across asterids. Future investigations that contrast

580 the ancestral and modern states of NRC proteins will provide valuable insights into the

581 biochemical function of NLR pairs and networks in plants and how these have evolved over

582 125 million years.

583

584 **Materials and Methods**

585

586 **Phylogenetic analyses**

587

588 For the phylogenetic analysis, we aligned NLR amino acid sequences using MAFFT v.7 (Katoh

589 and Standley, 2013) and deleted the gaps in the alignments by our own Python script. The script

590 is available from GitHub (https://github.com/slt666666/NRC0). NB-ARC domain sequences

591 of the aligned NLR datasets were used for generating phylogenetic trees. The maximum

592 likelihood phylogenetic tree was generated in RAxML version 8.2.12 with JTT model and

593 bootstrap values based on 100 iterations. All datasets used for phylogenetic analyses are in

594 Supplemental Files 13-18.

595

596 **Patristic distance analyses**

597

598 To calculate the phylogenetic (patristic) distance, we used Python script based on DendroPy

599 (Sukumaran and Mark, 2010). We calculated patristic distances from each NRC to the other

600 NRCs on the phylogenetic tree (Supplemental File 13) and extracted the distances between

601 NRCs of tomato to the closest NRC from the other plant species. The script used for the

602 patristic distance calculation is available at GitHub (https://github.com/slt666666/NRC0).

603

604 **Gene cluster analysis**

605

606 To calculate the genetic distances, we extracted gene annotation data from NCBI database as

607 gff3 format. The genetic distances between NLR genes were calculated by our own Python

608 script. The script is available from GitHub (https://github.com/slt666666/NRC0). We defined

609 NLR clusters as NLR sets that genetic distances are less than 50 kb apart from each other. NLR

610 clusters were visualized in phylogenetic tree by iTOL (Letunic and Bork., 2021). To visualize

611   phylogenetic relationships of clustered NLRs in each specie, we developed "gene-cluster-

612   matrix" library (https://github.com/slt666666/gene-cluster-matrix).

613

614   **NRC0 and its sensor candidate sequence retrieval**

615

616   We performed BLAST (Altschul et al., 1990) using amino acid sequences of NRC0 orthologs

617   from carrot (DCAR_023561), coffee (Cc11_g06560), wild sweet potato (itf14g00240.t1 and

618   itf14g00270.t1), and tomato (Solyc10g008220.4.1) as queries to search NRC0-like sequences

619   in NCBI nr or nr/nt database (https://blast.ncbi.nlm.nih.gov/Blast.cgi). In the BLAST search,

620   we used cut-offs, percent identity $\geq$ 40% and query coverage $\geq$ 95%. NB-ARC domain

621   sequences of the aligned sequences of the BLAST result were used for generating a

622   phylogenetic tree and extracted NLRs located in the NRC0 clade as NRC0-like sequences. The

623   BLAST pipeline was circulated by using the obtained sequences as new queries to search

624   NRC0-like sequences over the angiosperm species.

625

626   We also generated a phylogenetic tree of NLR dataset of each specie, in which NRC0-like

627   sequences were found and extracted NLRs located in the NRC0 clade as NRC0-like sequences.

628   Finally, we generated a phylogenetic tree of NRC0-like sequences and NLR dataset of six

629   asterid species (*Nyssa sinensis, Camellia sinensis, Cynara cardunculus, Daucus carota,*

630   *Sesamum indicum, Solanum lycopersicum*) and defined NRC0 ortholog clade that include

631   NRC0 sequences of carrot, coffee, wild sweet potato, and tomato based on phylogenetically

632   well-supported bootstrap value. To extract *NRC0-S* gene, we extracted genes located within 50

633   kb from obtained *NRC0* genes and ran the NLR tracker pipeline (Kourelis et al., 2021) to

634   annotate NLR genes among them.

635

636   **Sequence conservation analyses**

637

638   Full-length amino acid sequences of the NRC0 or NRC0-S were subjected to motif searches

639   using the MEME (Multiple EM for Motif Elicitation) (Bailey and Elkan, 1994) with parameters

640   'zero or one occurrence per sequence, top twenty motifs', to detect consensus motifs conserved

641   in $\geq$90% of the input sequences. The output data are summarized in Supplemental Table S4

642   and S5.

643

644   To analyze amino acid sequence conservation and variation in NRC0 or NRC0-S proteins,

645   aligned amino acid sequences of each NRC0 and NRC0-S datasets by MAFFT v.7 were used

646   for the ConSurf pipeline (Ashkenazy et al., 2016). Tomato NRC0 (XP_004248175.2) or

647   NRC0-Sa (XP_004248174.1) was used as a query for each analysis of NRC0 or NRC0-S,

648   respectively. The output datasets of the ConSurf analyses are in Supplemental Data Set 2 and

649   3.

650

651   **Plant growth condition**

652

653   Wild-type and mutant *Nicotiana benthamiana* were grown in a controlled growth chamber with

654   temperature 22–25°C, humidity 45–65% and 16/8 hr light/dark cycle. The *NRC* knockout lines

655   used have been previously described: *nrc2/3/4*-210.4.3 and *nrc2/3/4*-210.5.5 (Wu et al., 2020).

656

657   **Plasmid construction**

658

659   Wild-type and MHD-mutant variants of *NRC0* and *NRC0-S* from tomato (*S. lycoperiscum*, Sl-),

660   wild sweet potato (*I. trifida,* Itf-), coffee (*C. canephora* or *C. arabica,* Cc- or Ca-) and carrot

661   (*D. carota,* DCAR-) were synthesized in pICH41155 through GENEWIZ Standard Gene

662   Synthesis with synonymous mutations to *Bsa*I and *Bpi*I restriction enzyme sites. The

663   synthesized genes were assembled into the binary vector pICH47732 or pICH47751 from the

664   Golden Gate Modular Cloning (MoClo) kit (Weber et al, 2011) together with pICH51266 (35S

665   promoter) and pICH41432 (OCS terminator) from the MoClo plant parts kit (Engler et al,

666   2014).

667

668   For BN-PAGE experiment, the MADA motif mutant of *SlNRC0* was amplified by Phusion

669   High-Fidelity   DNA   Polymerase   (Thermo   Fisher)   with   forward   mutation   primer

670   (AATGGTCTCTAATGGCTGATGCTGTTGTCGAATTTGAATTGTTAAATGAGAAAC

671   AACTAGAACTTTATCATGTGGATTTG)   and   reverse   primer

672   (AATGGTCTCTCGAACCAATATCTGGAGGATAGATGAC). The purified amplicon was

673   used for Golden Gate assembly with pICSL50007 (3xFLAG) into the binary vector pICH86988

674   (level 1 acceptor with 35S promoter and OCS terminator). The synthetic *SlNRC0-Sa^{DV}* was

675   also assembled into the pICH86988 binary vector, together with pICSL50009 (6xHA). *Rx* and

676   *NRC2^{EEE}* constructs used were described previously (Contreras et al., 2023), and were

677   assembled into the pJK268c vector with C-terminal tag modules pICSL50012 (V5) and

678   pICSL50007 (3xFLAG), respectively.

679

680   Plasmid information is described in Supplemental File 19.

681

682   **Transient gene expression and cell death assays**

683

684   Transient gene expression in *N. benthamiana* leaves was performed by agroinfiltration
685   according to methods described previously (Bos et al., 2006). Briefly, four-week-old *N.*
686   *benthamiana* plants were infiltrated with *Agrobacterium* Gv3101 strains carrying the binary
687   expression plasmids. The *Agrobacterium* suspensions were prepared in infiltration buffer (10
688   mM MES, 10 mM MgCl$_2$, and 150 μM acetosyringone, pH 5.6). To overexpress NLRs for cell
689   death assays, the concentration of each suspension was adjusted to OD$_{600}$ = 0.25. Macroscopic
690   cell death phenotypes were scored according to the scale of Adachi et al. (2023).

691

692   **Protein extraction and BN-PAGE assay**

693

694   Four-week-old *nrc2/3/4* plants were infiltrated with *Agrobacterium* suspensions as the
695   concentration of each suspension is indicated in Supplemental File 19. Leaf tissue was
696   collected at 72 hours after agroinfiltration in liquid nitrogen and was grounded in a
697   Geno/Grinder homogenizer. Total proteins were extracted in GTMN buffer [10% glycerol, 50
698   mM tris-HCl (pH 7.5), 5 mM MgCl$_2$, and 50 mM NaCl] supplemented with 10 mM
699   dithiothreitol (DTT), 1x protease inhibitor cocktail (Sigma-Aldrich) and 0.2% Triton X-100
700   (Sigma-Aldrich), and incubated on ice for 10 min. After centrifugation at 5000 x*g* for 15 min,
701   supernatants were used for BN-PAGE and SDS-PAGE assays.

702

703   For BN-PAGE, 25 μl of extracted protein samples were mixed with NativePAGE 5% G-250
704   sample additive (Invitrogen). 5 μl of each sample was loaded to NativePAGE 4 to 16% bis-tris
705   gels (Invitrogen). Proteins were transferred to PVDF membranes with NuPAGE Transfer
706   Buffer (Invitrogen) in a Trans-Blot Turbo transfer apparatus (Bio-Rad) by following the
707   manufacturer's instruction. Proteins were fixed to the membranes by incubating with 8% acetic
708   acid for 15 min and were left to dry. For SDS-PAGE, extracted proteins were diluted in SDS
709   loading dye and incubated at 72°C for 10 min and were loaded to 4-20% Mini-PROTEAN
710   TGX gels (Bio-Rad). Immunoblotting was performed with antibodies: anti-hemagglutinin
711   (HA) (3F10) HRP (Roche), anti-V5 (V2260) HRP (Roche) and anti-FLAG (M2) (Sigma) in a
712   1:5000 dilution.

713

Accession numbers

715

Genome and gene information used in this study can be found from reference genome or GenBank/EMBL databases with accession numbers listed in Supplemental Data Set 5, Tables S1 and S3.

719

Supplemental Data

721

Supplemental Figure S1. Phylogenetic tree of NRC-H clade of six asterid species.

Supplemental Figure S2. Clustered NLRs of four asterid species.

Supplemental Figure S3. Quantification of the autoactive cell death response triggered by multiple combinations of NRC0 and NRC0-S.

726

Supplemental Table S1. List of *NRC0* and *NRC0-S*.

Supplemental Table S2. List of NLR gene cluster in four asterid species.

Supplemental Table S3. List of NRC in 31 asterids and 1 Caryophyllales species.

Supplemental Table S4. List of MEME motifs predicted from NRC0.

Supplemental Table S5. List of MEME motifs predicted from NRC0-S.

732

Supplemental Data Set 1. NLR gene cluster matrix files of four asterid species used for Supplemental Figure S2.

Supplemental Data Set 2. The ConSurf conservation score among NRC0 proteins.

Supplemental Data Set 3. The ConSurf conservation score among NRC0-S proteins.

Supplemental Data Set 4. Summary of HR index scores in cell death assay.

Supplemental Data Set 5. Reference genome databases used for NLR annotations.

739

Supplemental File 1. Amino acid sequences of NLRs in six asterid species and functionally validated NLRs used for Figure 1A.

Supplemental File 2. Amino acid alignment file of the NB-ARC domain of NLRs in six asterid species and functionally validated NLRs used for Figure 1A.

Supplemental File 3. Amino acid sequences of NLRs in four asterid species and functionally validated NLRs used for Figure 2A.

Supplemental File 4. Amino acid alignment file of the NB-ARC domain of NLRs in four

747   asterid species and functionally validated NLRs used for Figure 2A.

748   **Supplemental File 5.** Amino acid sequences of CC-NLRs in six asterid species, NRC0, and

749   NRC0-S used for Figure 3B.

750   **Supplemental File 6.** Amino acid alignment file of the NB-ARC domain of CC-NLRs in six

751   asterid species, NRC0, and NRC0-S used for Figure 3B.

752   **Supplemental File 7.** Amino acid sequences of NRC helpers used for Figure 4A.

753   **Supplemental File 8.** Amino acid alignment file of full-length NRC helpers used for Figure

754   4A.

755   **Supplemental File 9.** Amino acid sequences of NRC0.

756   **Supplemental File 10.** Amino acid sequences of NRC0-S.

757   **Supplemental File 11.** Amino acid alignment file of NB-ARC domains and phylogenetic tree

758   file of each of 31 asterid species and 1 Caryophyllales species used for Figure 4B.

759   **Supplemental File 12.** Amino acid sequences of NRCs in 31 asterid species and 1

760   Caryophyllales species.

761   **Supplemental File 13.** NLR phylogenetic tree file in Figure 1A.

762   **Supplemental File 14.** NLR phylogenetic tree file in Supplemental Figure S1.

763   **Supplemental File 15.** NLR phylogenetic tree file in Figure 2A.

764   **Supplemental File 16.** NLR phylogenetic tree file in Supplemental Figure S2.

765   **Supplemental File 17.** NLR phylogenetic tree file in Figure 3B.

766   **Supplemental File 18.** NLR phylogenetic tree file in Figure 4A.

767   **Supplemental File 19.** Plasmid list used in this study.

768

769

770   **ACKNOWLEDGEMENTS**

771

781   sabbatical year at TSL.

782

783

784   **AUTHOR CONTRIBUTIONS**

785

786   Conceptualization: S.K., C.H.W., H.A.; Data curation: T.S., C.M.-A., M.P.C.; Formal analysis:

787   T.S., C.M.-A., M.P.C., H.A.; Investigation: T.S., C.M.-A., M.P.C., H.A.; Methodology: T.S.,

788   C.M.-A., M.P.C., H.A.; Resources: T.S., M.P.C., C.H.W., H.A.; Software: T.S.; Supervision:

789   S.K., H.A.; Funding acquisition: S.K., H.A.; Project administration: S.K., H.A.; Writing initial

790   draft: T.S., H.A.; Editing: T.S., C.M.-A., M.P.C., S.K., C.H.W., H.A.

791

792

793   **DECLARATION OF INTERESTS**

794

795   S.K. receives funding from industry on NLR biology and is a co-founder of start-up companies

796   that focus on plant disease resistance. M.P.C. and S.K. have filed patents on NLR biology.

797   M.P.C. has received fees from Resurrect Bio Ltd, a start-up company related to NLR biology.

798

799

800   **References**

801

802   **Adachi H, Contreras MP, Harant A, Wu CH, Derevnina L, Sakai T, Duggan C, Moratto E, Bozkurt TO,**

803   **Maqbool A, et al.** An N-terminal motif in NLR immune receptors is functionally conserved across distantly

804   related plant species. *eLife.* 2019a:**8**:e49956.

805   **Adachi H, Derevnina L, Kamoun S.** NLR singletons, pairs, and networks: evolution, assembly, and regulation

806   of the intracellular immunoreceptor circuitry of plants. *Curr Opin Plant Biol.* 2019b:50:121-131.

807   **Adachi H, Kamoun S.** NLR receptor networks in plants. *Essays Biochem.* 2022:66(5):541-549.

808   **Adachi H, Sakai T, Kourelis J, Pai H, Gonzalez Hernandez JL, Utsumi Y, Seki M, Maqbool A, Kamoun S.**

809   Jurassic NLR: conserved and dynamic evolutionary features of the atypically ancient immune receptor ZAR1.

810   *Plant Cell.* 2023:koad175.

811   **Ahn HK, Lin X, Olave-Achury AC, Derevnina L, Contreras MP, Kourelis J, Wu CH, Kamoun S, Jones**

812   **JDG.** Effector-dependent activation and oligomerization of plant NRC class helper NLRs by sensor NLR

813   immune receptors Rpi-amr3 and Rpi-amr1. *EMBO J.* 2023:42(5):e111484.

814   **Altschul SF, Gish W, Miller W, Myers EW, Lipman DJ.** Basic local alignment search tool. *J Mol Biol.*

815   1990:215(3):403-410.

816   **Ashkenazy H, Abadi S, Martz E, Chay O, Mayrose I, Pupko T, Ben-Tal N.** ConSurf 2016: an improved

817   methodology to estimate and visualize evolutionary conservation in macromolecules. *Nucleic Acids Res.*
818   2016:44(W1):W344-W350.

819   **Baggs E, Dagdas G, Krasileva KV.** NLR diversity, helpers and integrated domains: making sense of the NLR
820   IDentity. *Curr Opin Plant Biol.* 2017:38:59-67.

821   **Baggs EL, Monroe JG, Thanki AS, O'Grady R, Schudoma C, Haerty W, Krasileva KV.** Convergent loss of
822   an EDS1/PAD4 signaling pathway in several plant lineages reveals coevolved components of plant immunity
823   and drought response. *Plant Cell.* 2020:32(7):2158-2177.

824   **Bailey TL, Elkan C.** Fitting a mixture model by expectation maximization to discover motifs in biopolymers.
825   *Proc Int Conf Intell Syst Mol Biol.* 1994:2:28-36.

826   **Barragan AC, Weigel D.** Plant NLR diversity: the known unknowns of pan-NLRomes. *Plant Cell.*
827   2021:33(4):814-831.

828   **Bendahmane A, Farnham G, Moffett P, Baulcombe DC.** Constitutive gain-of-function mutants in a nucleotide
829   binding site–leucine rich repeat protein encoded at the *Rx* locus of potato. *Plant J.* 2002:32(2):195-204.

830   **Bi G, Su M, Li N, Liang Y, Dang S, Xu J, Hu M, Wang J, Zou M, Deng Y, et al.** The ZAR1 resistosome is a
831   calcium-permeable channel triggering plant immune signaling. *Cell.* 2021:184(13):3528-3541.e12.

832   **Bos JI, Kanneganti TD, Young C, Cakir C, Huitema E, Win J, Armstrong MR, Birch PR, Kamoun S.** The
833   C-terminal half of *Phytophthora infestans* RXLR effector AVR3a is sufficient to trigger R3a-mediated
834   hypersensitivity and suppress INF1- induced cell death in *Nicotiana benthamiana. Plant J.* 2006:48(2):165-
835   176.

836   **Césari S, Kanzaki H, Fujiwara T, Bernoux M, Chalvon V, Kawano Y, Shimamoto K, Dodds P, Terauchi
837   R, Kroj T.** The NB-LRR proteins RGA4 and RGA5 interact functionally and physically to confer disease
838   resistance. *EMBO J.* 2014:33(17):1941-1959.

839   **Contreras MP, Pai H, Tumtas Y, Duggan C, Yuen ELH, Cruces AV, Kourelis J, Ahn HK, Lee KT, Wu CH,
840   et al.** Sensor NLR immune proteins activate oligomerization of their NRC helpers in response to plant
841   pathogens. *EMBO J.* 2023a:42(5):e111519.

842   **Contreras MP, Pai H, Selvaraj M, Toghani A, Lawson DM, Tumtas Y, Duggan C, Yuen ELH, Stevenson
843   CEM, Harant A, et al.** Resurrection of plant disease resistance proteins via helper NLR bioengineering. *Sci
844   Adv.* 2023b;9(18):eadg3861.

845   **Dong OX, Ao K, Xu F, Johnson KCM, Wu Y, Li L, Xia S, Liu Y, Huang Y, Rodriguez E, et al.** Individual
846   components of paired typical NLR immune receptors are regulated by distinct E3 ligases. *Nat Plants.*
847   2018:4(9):699-710.

848   **Duggan C, Moratto E, Savage Z, Hamilton E, Adachi H, Wu CH, Leary AY, Tumtas Y, Rothery SM,
849   Maqbool A, et al.** Dynamic localization of a helper NLR at the plant-pathogen interface underpins pathogen
850   recognition. *Proc Natl Acad Sci U S A.* 2021:118(34):e2104997118.

851   **Engler C, Youles M, Gruetzner R, Ehnert TM, Werner S, Jones JD, Patron NJ, Marillonnet S.** A golden
852   gate modular cloning toolbox for plants. *ACS synthetic biology.* 2014:3(11):839–843.

853   **Eddy SR.** Profile hidden markov models. *Bioinformatics.* 1998:14(9):755-763.

854   **Förderer A, Li E, Lawson AW, Deng YN, Sun Y, Logemann E, Zhang X, Wen J, Han Z, Chang J, et al.** A
855   wheat resistosome defines common principles of immune receptor channels. *Nature.* 2022:610(7932):532-539.

856   **Gong Z, Qi J, Hu M, Bi G, Zhou JM, Han GZ.** The origin and evolution of a plant resistosome. *Plant Cell.*

857   2022:34(5):1600-1620.

858   **Jones JD, Vance RE, Dangl JL.** Intracellular innate immune surveillance devices in plants and animals. *Science.*
859   2016:354(6316):aaf6395.

860   **Karasov TL, Chae E, Herman JJ, Bergelson J.** Mechanisms to mitigate the trade-off between growth and
861   defense. *Plant Cell.* 2017:29(4):666-680.

862   **Katoh K, Standley DM.** MAFFT multiple sequence alignment software version 7: improvements in performance
863   and usability. *Mol Biol Evol.* 2013:30(4):772-780.

864   **Kibby EM, Conte AN, Burroughs AM, Nagy TA, Vargas JA, Whalen LA, Aravind L, Whiteley AT.**
865   Bacterial NLR-related proteins protect against phage. *Cell.* 2023:186(11):2410-2424.e18.

866   **Kourelis J, Malik S, Mattinson O, Krauter S, Kahlon PS, Paulus JK, van der Hoorn RAL.** Evolution of a
867   guarded decoy protease and its receptor in solanaceous plants. *Nature Commun.* 2020:11(1):4393.

868   **Kourelis J, Sakai T, Adachi H, Kamoun S.** RefPlantNLR is a comprehensive collection of experimentally
869   validated plant disease resistance proteins from the NLR family. *PLoS Biol.* 2021:19(10):e3001124.

870   **Kourelis J, Adachi H.** Activation and regulation of NLR immune receptor networks. *Plant Cell Physiol.*
871   2022:63(10):1366-1377.

872   **Kourelis J, Contreras MP, Harant A, Pai H, Lüdke D, Adachi H, Derevnina L, Wu CH, Kamoun S.** The
873   helper NLR immune protein NRC3 mediates the hypersensitive cell death caused by the cell-surface receptor
874   Cf-4. *PLoS Genet.* 2022:18(9):e1010414.

875   **Lee HY, Mang H, Choi E, Seo YE, Kim MS, Oh S, Kim SB, Choi D.** Genome-wide functional analysis of hot
876   pepper immune receptors reveals an autonomous NLR clade in seed plants. *New Phytol.* 2021:229(1):532-547.

877   **Lee RRQ, Chae E.** Variation patterns of NLR clusters in *Arabidopsis thaliana* genomes. *Plant Commun.*
878   2020:1(4):100089.

879   **Le Roux C, Huet G, Jauneau A, Camborde L, Trémousaygue D, Kraut A, Zhou B, Levaillant M, Adachi
880   H, Yoshioka H, et al.** A receptor pair with an integrated decoy converts pathogen disabling of transcription
881   factors to immunity. *Cell.* 2015:161(5):1074-1088.

882   **Letunic I, Bork P.** Interactive Tree Of Life (iTOL) v5: an online tool for phylogenetic tree display and annotation.
883   *Nucleic Acids Res.* 2021:49(W1):W293-W296.

884   **Li J, Huang H, Zhu M, Huang S, Zhang W, Dinesh-Kumar SP, Tao X.** A plant immune receptor adopts a
885   two-step recognition mechanism to enhance viral effector perception. *Mol Plant.* 2019:12(2):248-262.

886   **Liang W, van Wersch S, Tong M, Li X.** TIR-NB-LRR immune receptor SOC3 pairs with truncated TIR-NB
887   protein CHS1 or TN2 to monitor the homeostasis of E3 ligase SAUL1. *New Phytol.* 2019:221(4):2054-2066.

888   **Liu Y, Zeng Z, Zhang YM, Li Q, Jiang XM, Jiang Z, Tang JH, Chen D, Wang Q, Chen JQ, et al.** An
889   angiosperm *NLR* Atlas reveals that *NLR* gene reduction is associated with ecological specialization and signal
890   transduction component deletion. *Mol Plant.* 2021:14(12):2015-2031.

891   **Maqbool A, Saitoh H, Franceschetti M, Stevenson CE, Uemura A, Kanzaki H, Kamoun S, Terauchi R,
892   Banfield MJ.** Structural basis of pathogen recognition by an integrated HMA domain in a plant NLR immune
893   receptor. *elife.* 2015:4:e08709.

894   **Michelmore RW, Meyers BC.** Clusters of resistance genes in plants evolve by divergent selection and a birth-
895   and-death process. *Genome Res.* 1998:8(11):1113-1130.

896   **Narusaka M, Shirasu K, Noutoshi Y, Kubo Y, Shiraishi T, Iwabuchi M, Narusaka Y.** *RRS1* and *RPS4* provide

897   a dual *Resistance*-gene system against fungal and bacterial pathogens. *Plant J.* 2009:60(2):218-226.

898   **Prigozhin DM, Krasileva KV.** Analysis of intraspecies diversity reveals a subset of highly variable plant immune

899   receptors and predicts their binding sites. *Plant Cell.* 2021:33(4):998-1015.

900   **Sarris PF, Duxbury Z, Huh SU, Ma Y, Segonzac C, Sklenar J, Derbyshire P, Cevik V, Rallapalli G, Saucet**

901   **SB, et al.** A plant immune receptor detects pathogen effectors that target WRKY transcription factors. *Cell.*

902   2015:161(5):1089-1100.

903   **Saur IM, Conlan BF, Rathjen JP.** The N-terminal domain of the tomato immune protein prf contains multiple

904   homotypic and pto kinase interaction sites. *J Biol Chem.* 2015:290(18):11258-11267.

905   **Seong K, Seo E, Witek K, Li M, Staskawicz B.** Evolution of NLR resistance genes with noncanonical N-terminal

906   domains in wild tomato species. *New Phytol.* 2020:227(5):1530-1543.

907   **Shao ZQ, Xue JY, Wu P, Zhang YM, Wu Y, Hang YY, Wang B, Chen JQ.** Large-scale analyses of angiosperm

908   nucleotide-binding site-leucine-rich repeat genes reveal three anciently diverged classes with distinct

909   evolutionary patterns. *Plant Physiol.* 2016:170(4):2095-2109.

910   **Shimizu M, Hirabuchi A, Sugihara Y, Abe A, Takeda T, Kobayashi M, Hiraka Y, Kanzaki E, Oikawa K,**

911   **Saitoh H, et al.** A genetically linked pair of NLR immune receptors shows contrasting patterns of evolution.

912   *Proc Natl Acad Sci U S A.* 2022:119(27):e2116896119.

913   **Smith SA, Brown JW.** Constructing a broadly inclusive seed plant phylogeny. *Am J Bot.* 2018:105(3):302-314.

914   **Sugihara Y, Abe Y, Takagi H, Abe A, Shimizu M, Ito K, Kanzaki E, Oikawa K, Kourelis J, Langner T, et**

915   **al. 2023.** Disentangling the complex gene interaction networks between rice and the blast fungus identifies a

916   new pathogen effector. *PLoS Biol.* 2023:21(1):e3001945.

917   **Sukumaran J, Holder MT.** DendroPy: a Python library for phylogenetic computing. *Bioinformatics.*

918   2010:26(12):1569-1571.

919   **Uehling J, Deveau A, Paoletti M.** Do fungi have an innate immune response? An NLR-based comparison to

920   plant and animal immune systems. *PLoS Pathog.* 2017:13(10):e1006578.

921   **Van de Weyer AL, Monteiro F, Furzer OJ, Nishimura MT, Cevik V, Witek K, Jones JDG, Dangl JL, Weigel**

922   **D, Bemm F.** A species-wide inventory of NLR genes and alleles in *Arabidopsis thaliana*. *Cell.*

923   2019:178(5):1260-1272.e14.

924   **Wang J, Wang J, Hu M, Wu S, Qi J, Wang G, Han Z, Qi Y, Gao N, Wang H-W, et al.** Ligand-triggered

925   allosteric ADP release primes a plant NLR complex. *Science.* 2019a:364(6435):eaav5868.

926   **Wang J, Hu M, Wang J, Qi J, Han Z, Wang G, Qi Y, Wang H-W, Zhou J-M, Chai J.** Reconstitution and

927   structure of a plant NLR resistosome conferring immunity. *Science.* 2019b:364(6435):eaav5870.

928   **Weber E, Engler C, Gruetzner R, Werner S, Marillonnet S.** A modular cloning system for standardized

929   assembly of multigene constructs. *PLoS One*. 2011:6(2):e16765.

930   **Wikström N, Kainulainen K, Razafimandimbison SG, Smedmark JE, Bremer B.** A revised time tree of the

931   asterids: establishing a temporal framework for evolutionary studies of the coffee family (rubiaceae). *PLoS One.*

932   2015:10(5):e0126690.

933   **Wu CH, Abd-El-Haliem A, Bozkurt TO, Belhaj K, Terauchi R, Vossen JH, Kamoun S.** NLR network

934   mediates immunity to diverse plant pathogens. *Proc Natl Acad Sci U S A.* 2017:114(30):8113-8118.

935   **Wu CH, Adachi H, De la Concepcion JC, Castells-Graells R, Nekrasov V, Kamoun S.** *NRC4* gene cluster is

936   not essential for bacterial flagellin-triggered immunity. *Plant Physiol.* 2020:182(1):455-459.

937   **Xu F, Zhu C, Cevik V, Johnson K, Liu Y, Sohn K, Jones JD, Holub EB, Li X.** Autoimmunity conferred by
938   *chs3-2D* relies on *CSA1*, its adjacent TNL-encoding neighbour. *Sci Rep.* 2015:5:8792.

939   **Yang Y, Kim NH, Cevik V, Jacob P, Wan L, Furzer OJ, Dangl JL.** Allelic variation in the *Arabidopsis* TNL
940   CHS3/CSA1 immune receptor pair reveals two functional cell-death regulatory modes. *Cell Host Microbe.*
941   2022:30(12):1701-1716.e5.

942   **Zhang N, Gan J, Carneal L, González-Tobón J, Filiatrault M, Martin GB.** Helper NLRs Nrc2 and Nrc3 act
943   co-dependently with Prf/Pto and activate MAPK signaling to induce immunity in tomato. *biorxiv.* 2023. doi:
944   https://doi.org/10.1101/2023.08.17.553711.

945   **Zhang Y, Wang Y, Liu J, Ding Y, Wang S, Zhang X, Liu Y, Yang S.** Temperature-dependent autoimmunity
946   mediated by *chs1* requires its neighboring TNL gene *SOC3*. *New Phytol.* 2017:213(3):1330-1345.

947

Tree scale 0.2: ⊢———⊣ ▶ : Bootstrap > 70

948

949

950 **Supplemental Figure S1. Phylogenetic tree of NRC-H clade of six asterid species.** The maximum
951 likelihood phylogenetic tree was generated in RAxML version 8.2.12 with JTT model using NB-ARC
952 domain sequences of 83 NRC-Hs identified from carrot, monkey flower, coffee, wild sweet potato, *Nicotiana*
953 *benthamiana*, and tomato. Red arrow heads indicate bootstrap support > 0.7. The scale bars indicate the
954 evolutionary distance in amino acid substitution per site.

955
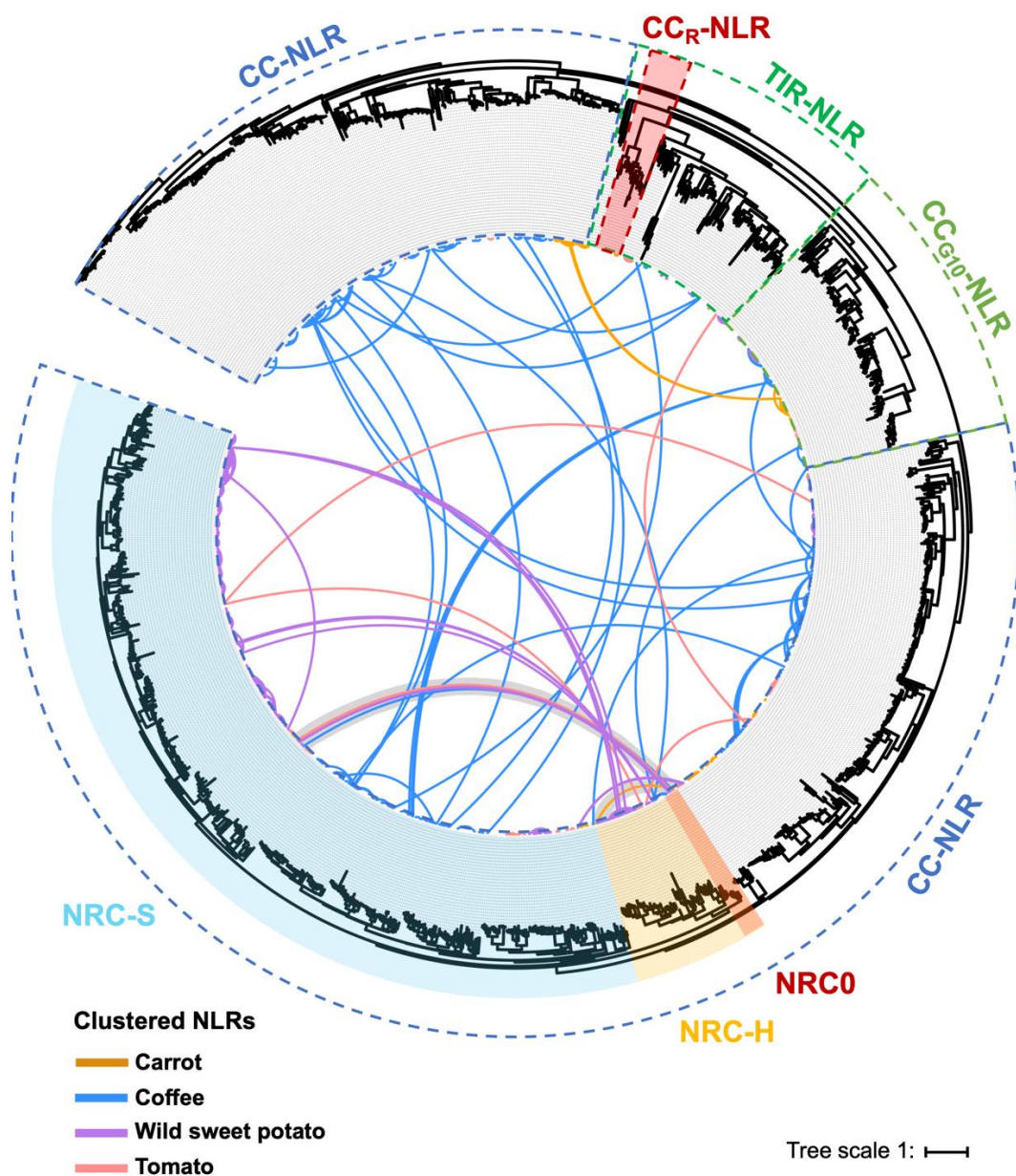
Supplemental Figure S2. Genetically clustered NLRs in four asterid species. The maximum likelihood phylogenetic tree was generated in RAxML version 8.2.12 with JTT model using NB-ARC domain sequences of 1,265 NLRs identified from carrot, coffee, wild sweet potato and tomato. The NRC superclade containing NRC0, NRC-H, and NRC-S clades are described with different background colors. The connected lines inside the phylogenetic tree indicate genetic link between NLR genes (distance < 50 kb) with different colors based on plant species. Gray band indicate genetic link between *NRC0* and *NRC0-S*.
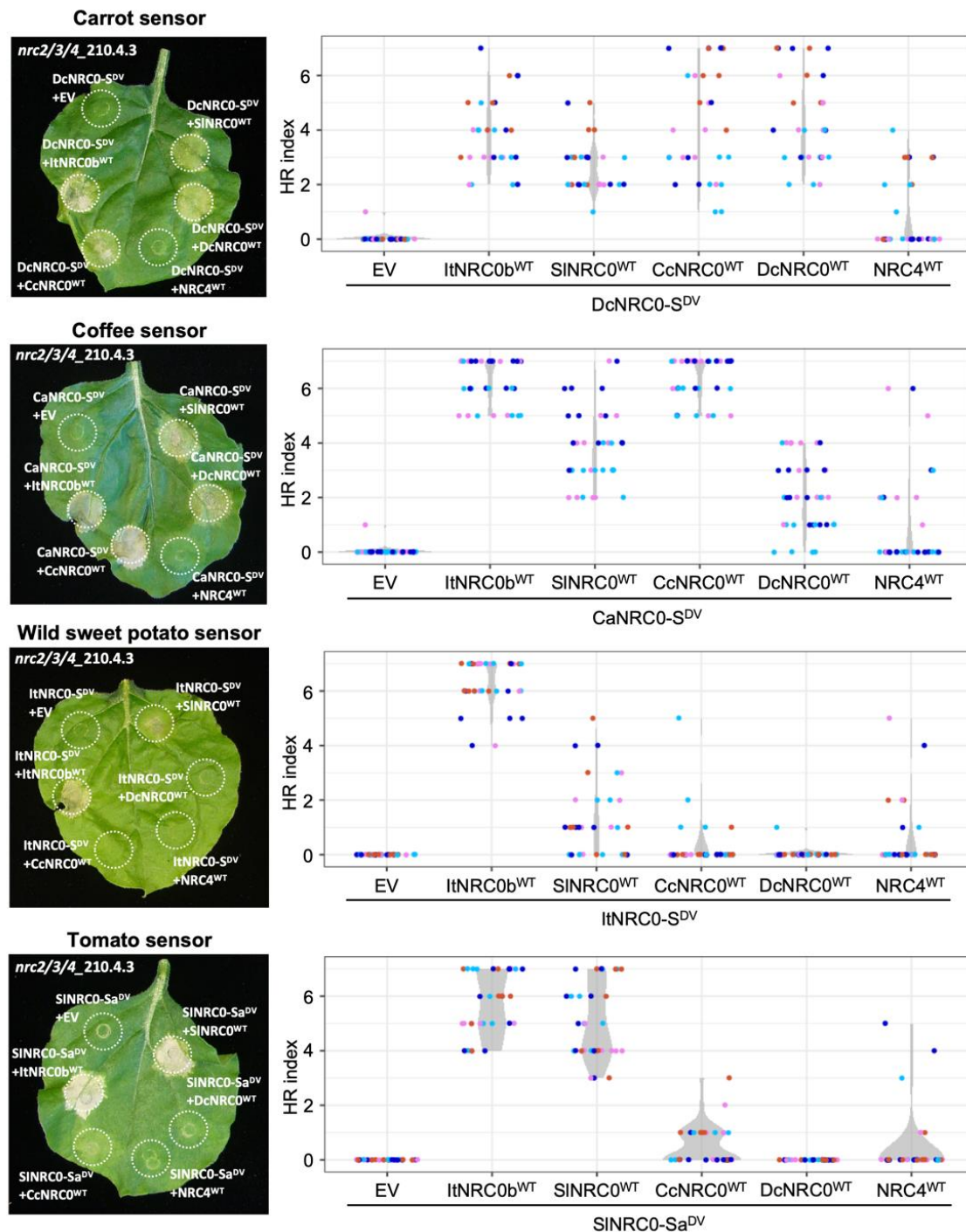
Supplemental Figure S3. Quantification of the autoactive cell death response triggered by multiple combinations of NRC0 and NRC0-S. Left images are identical to representative images of autoactive cell death shown in Figure 7. Violin plots describe cell death intensity scored as an HR index based on three or four independent experiments.